ISSN 1028-8546

Volume XXII, Number 2
Section: En
July, 2016

Azerbaijan Journal of Physics

Fizika

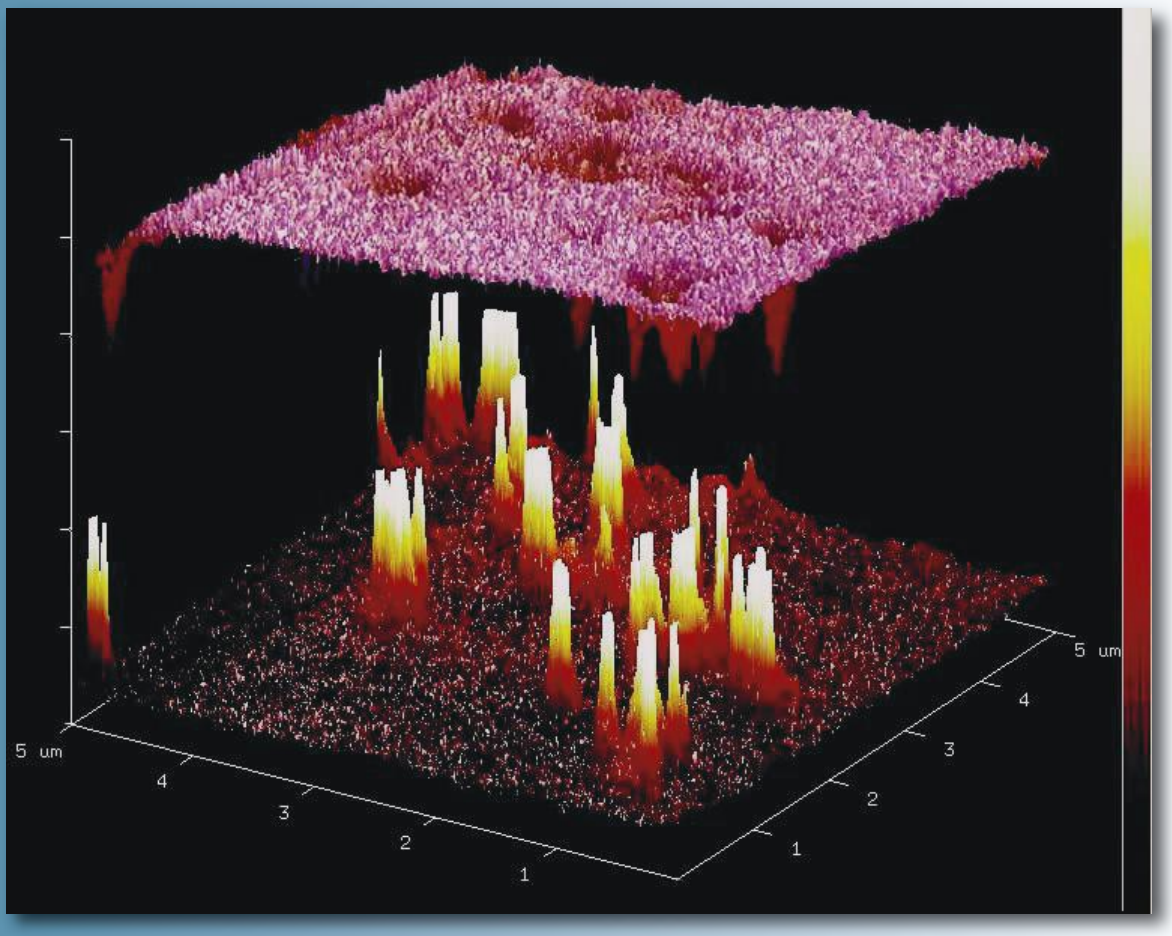

www.physics.gov.az

G.M. Abdullayev Institute of Physics
Azerbaijan National Academy of Sciences
Department of Physical, Mathematical and Technical Sciences

Published from 1995
Ministry of Press and Information
of Azerbaijan Republic,
Registration number 402, 16.04.1997

ISSN 1028-8546
vol. XXII, Number 02, 2016
Series: En

Azerbaijan Journal of Physics

FIZIKA

G.M.Abdullayev Institute of Physics
Azerbaijan National Academy of Sciences
Department of Physical, Mathematical and Technical Sciences

PUBLISHING OFFICE

131 H.Javid ave, AZ-1143, Baku
ANAS, G.M.Abdullayev Institute of Physics

Tel.: (99412) 539-51-63, 539-32-23
Fax: (99412) 447-04-56
E-mail: jophphysics@gmail.com
Internet: www.physics.gov.az

It is authorized for printing:

Published at "**SƏRQ-QƏRB**"
17 Ashug Alessger str., Baku
Typographer : Aziz Gulaliyev

Sent for printing on: __.__. 201_
Printing approved on: __.__. 201_
Physical binding:_____
Number of copies:_____200
Order:_____

TRAPPING OF SLOW-SPEED PARTICLES IN A GAS CELL BY NONHOMOGENEOUS ELECTROMAGNETIC FIELDS INTENSIFYING WITH TIME

AZAD Ch. IZMAILOV
Institute of Physics, Azerbaijan National Academy of Sciences,
Javid av. 131, Baku, Az-1143, Azerbaijan
email: azizm57@rambler.ru

We analyze possibilities of new trapping method of comparatively slow-speed classical particles in the potential well induced by the nonhomogeneous electromagnetic field increasing with time (up to some moment). It is assumed that given particles are contained in a cell in the high vacuum and acting upon them forces are not dissipative. This trapping method is especially effective at inelastic collisions of particles with walls of the cell when necessary preliminary slowdown of particles is possible for their following capture even to a highly shallow potential well. Corresponding sufficiently compact and simple electromagnetic traps may be used for capture and accumulation not only slow-speed micro- and nano-particles in the high vacuum but also atoms and molecules in the ground quantum state.

Keywords: electromagnetic potential well, classical particles, gas cell, inelastic collisions.
PACS: 45.50.-j, 41.20.-q, 42.50.Wk, 42.62.Fi

1. INTRODUCTION

Electromagnetic traps of micro- and nanoparticles in the high vacuum open new possibilities for contactless measurements of forces acting on given particles with extremely high accuracy and also allow micromanipulations of such particles, for example, in hollow waveguides [1]. Even more important is the development of effective methods of trapping and localization of sufficiently slow-speed atoms and molecules, in particular, for ultrahigh resolution spectroscopy [2] and for creation of more precise standards of time and frequency [3].

In papers [4,5] we have established the new trapping mechanism of comparatively slow-speed classical particles in electromagnetic potential wells which are induced by an electromagnetic field with a nondecreasing strength and fixed spatial distribution. We consider situations when given particles are contained in high the vacuum and acting upon them external forces are not dissipative (i.e. these particles move without friction). Depending on whether particles have electric (magnetic) moment, it is possible to use the controllable electric (magnetic) field or nonresonance laser radiation for their analyzed trapping.

In the present work we will show that efficiency of such a trapping mechanism essentially increases in cases of inelastic reflection of given particles from walls of the gas cell.

Then necessary preliminary slowdown of particles is possible for their following capture to the electromagnetic trap. Probability of such "cooling" collisions increases with time and therefore accumulation of trapped particles occurs during growth even a highly shallow potential well of the trap.

For visual demonstration of the proposed method, at first we will analyze the comparatively simple one-dimensional model of a cell and the electromagnetic trap with a gas of structureless particles (section 2).

Then we will discuss possible generalization of obtained results on real systems, including also atoms and molecules of rarefied gases (final section 3).

2. ONE-DIMENSIONAL MODEL OF THE TRAP

Let us consider a collection of noninteracting identical point-like particles, which are under conditions of the ultrahigh vacuum between plane-parallel walls of the one-dimensional cell with coordinates $x = \pm l$. We suppose that controllable electromagnetic field is superimposed on this cell, which creates the potential well for a particle described by the following function $U(x,t)$ of time t and coordinate x ($-l \le x \le l$):

$$U(x,t) = 0.5\, m\, \omega(t)^2 x^2 , \qquad (1)$$

where m is the particle mass and $\omega(t)$ is the positive value nondecreasing with time t. Corresponding motion equation of a particle in the well (1) is characteristic for the one-dimensional oscillator with the changing frequency $\omega(t)$:

$$\frac{d^2x}{dt^2} + \omega(t)^2 x = 0. \qquad (2)$$

Let us consider any particle, which reflects with a velocity $dx/dt = v_1$ from the cell wall with the coordinate $x = -l$. For example, we present the following time dependence $\omega(t)$:

$$\omega(t) = \omega_0 + \sigma \cdot t \cdot \eta(T - t) + \sigma \cdot T \cdot \eta(t - T), \quad (t \ge 0), \qquad (3)$$

where ω_0 is the value $\omega(t)$ in the initial moment t=0, $\sigma > 0$ is the constant parameter, $\eta(y)$ is the step function ($\eta(y) = 1$ if $y \ge 0$ and $\eta(y) = 0$ when $y < 0$), and T is the moment when growth of the frequency $\omega(t)$ stops and further $\omega(t) = (\omega_0 + \sigma \cdot T)$ is the constant. Fig.1 shows the example of the particle motion $x(t)$, calculated on the basis of the Eq.(2) with corresponding boundary conditions, at the change of the potential well (1) according to the time dependence (3). We see that, after reflection of the particle with a comparatively small velocity v_1 from the cell wall (with the coordinate

131 H.Javid ave, AZ-1143, Baku
ANAS, G.M.Abdullayev Institute of Physics
E-mail: jophphysics@gmail.com

$x = -l$), this particle does not reach the opposite wall (with the coordinate $x = l$) and turns back (in the point *z* in Fig.1) because of intensifying (with time) gradient force, which is directed to the center $x = 0$ of the potential well (1). Following motion of the particle is oscillations with the increasing frequency and decreasing amplitude up to the moment *t=T*, after which the value $\omega(t)$ (3) is constant. Then the particle undergoes usual harmonic oscillations (with the constant frequency and amplitude) already without collisions with cell walls (Fig.1). Thus it is possible to realize the trapping of sufficiently slow-speed particles by the nonhomogeneous electromagnetic field increasing with time (up to the definite moment). It is obvious, that such a trapping will not be possible for comparatively fast particles, which fly between cell walls overcoming the potential well (1).

Now we will determine the maximum velocity $v_1^*(t_1)$ of particles departing from a cell wall in some moment t_1, when given particles still may be captured in the electromagnetic trap. Corresponding analytical calculations may be carry out for adiabatic increase of the potential well (1), when a change of the frequency $\omega(t)$ is negligible during the characteristic oscillation period $2\pi/\omega(t)$ of a trapped particle, that is

$$\frac{2\pi}{\omega(t)}\,\frac{d\omega(t)}{dt} \ll \omega(t). \qquad (4)$$

Then, for any trapped particle in our one-dimensional model, the following adiabatic invariant is constant [6]:

$$I(t) = (m/2\pi)\int dv\,dx, \qquad (5)$$

where the two-dimensional integral is taken over the coordinate x and velocity v of a moving particle. Phase trajectory equation of such a particle for the potential well (1) has the known form:

$$0.5\,m\cdot v^2 + 0.5\,m\cdot\omega(t)^2\cdot x^2 = E(t,t_1), \qquad (6)$$

where $E(t,t_1)$ is the energy in the moment t for a particle, which is captured by the trap after reflection from any cell wall (with the coordinate $x = l$ or $-l$) in the moment $t_1 < t$. Then we receive the following adiabatic invariant (5) for such particles [6]:

$$I = E(t,t_1)/\omega(t). \qquad (7)$$

According to the invariant (7) and formula (6), the simple connection takes place between particle coordinate $x = l$ or $(-l)$ and its velocity v_1 in the moment t_1 of its reflection from a cell wall with corresponding values $x(t)$ and $v(t)$ in following moments $t > t_1$ of particle motion in the trap:

$$v(t)^2 + \omega(t)^2\cdot x(t)^2 = [\omega(t)/\omega(t_1)]\cdot v_1(t_1)^2 + \omega(t_1)\cdot\omega(t)\cdot l^2\,. \qquad (8)$$

At the adiabatic change of the frequency $\omega(t)$ (4), the first turn of a trapped particle (for example in the point *z* in Fig.1) after reflection from a wall in the moment t_1 occurs approximately in the moment $[t_1 + \pi/\omega(t_1)]$. The limitary initial velocity $v_1^*(t_1)$ for particles trapping is determined from the condition that such a particle touches the opposite wall of the cell (for example with the coordinate $x = l$ in Fig.1) in the indicated moment $[t_1 + \pi/\omega(t_1)]$. Thus, after substitution of values $v = 0$, $x^2 = l^2$ and $t = [t_1 + \pi/\omega(t_1)]$ in Eq.(8), we receive the following limitary velocity $v_1^*(t_1)$:

$$v_1^*(t_1) = l\cdot\sqrt{\omega(t_1)\,\{\omega[t_1 + \pi/\omega(t_1)] - \omega(t_1)\}} \approx l\cdot\sqrt{\pi\cdot\left(\frac{d\omega(t_1)}{dt_1}\right)}\,. \qquad (9)$$

We note that, in case of the stationary potential well (1), it is impossible to capture particles in such a trap because they will fly between walls of the cell even when their initial departure velocity (from a wall) is close to zero. It is confirmed also by the formula (9) where the velocity $v_1^* = 0$ for the constant value ω.

During sufficiently slow growth even a highly shallow potential well (1), it is possible to accumulate a large number of captured particles in this well if given particles are slowed up to velocities $v < v_1^*$ because of inelastic collisions with cell walls directly before their trapping. Indeed, let us analyze the case of the diffuse reflection of particles from a wall surface, after which the equilibrium (Maxwell) distribution $F(v)$ on particles velocities establishes [7]:

$$F(v) = \frac{1}{u\sqrt{\pi}}\,exp\left[-\left(\frac{v}{u}\right)^2\right], \qquad (10)$$

where $u = (2k_BT_w/m)^{0.5}$ is the most probable speed of free particles in the gas in the absence of the electromagnetic trap, k_B is the Boltzmann constant and T_w is the temperature of the cell walls. We will assume that the potential well (1) is so shallow that the relationship $\omega(t)\cdot l \ll u$ takes place and it is possible to neglect an electromagnetic trap influence on a distribution of comparatively fast particles which overcome the potential depth. Then the probability of capture of particles in the trap after their unitary collisions with cell walls in the moment *t* is determined by the value:

$$p(t) = 2\int_0^{v_1^*(t)} F(v)dv \approx \frac{2v_1^*(t)}{u\sqrt{\pi}}, \qquad (11)$$

where the limitary velocity $v_1^*(t)$ is determined by the formula (9) in case of the adiabatic growth of the potential well (1). A number of such trapped particles $N(t)$ in some cylindrical volume of our one-dimensional gas cell in the moment *t* has the form:

$$N(t) = 2l \cdot S \cdot n \cdot \theta(t), \qquad (12)$$

where S is the area of the corresponding part of cell walls in the selected volume, n is the equilibrium density of free particles in the absence of the electromagnetic trap, $\theta(t) \le 1$ is the fraction of trapped particles in the cell and $\theta(t=0) = 0$ in the initial moment t=0 of the trapping process. We receive the following balance equation on the basis of relationships (11) and (12):

$$\frac{dN(t)}{dt} = J \cdot p(t) \cdot [1 - \theta(t)] \cdot n \cdot S, \qquad (13)$$

where $J = 2\int_0^\infty F(v) \cdot v \cdot dv \approx 0.564\, u$, and $J \cdot [1-\theta(t)] \cdot n \cdot S$ is the flow of still nontrapped particles, which falls on the indicated part of cell walls with the area S in the moment t. Then from Eq. (11)-(13) we receive the fraction $\theta(t)$ of particles in the cell, which are captured in the electromagnetic trap up to the moment t:

$$\theta(t) = 1 - exp\left[-\frac{0.564}{l\cdot\sqrt{\pi}}\int_0^t v_1^*(t_1)\,d\,t_1\right]. \qquad (14)$$

In particular, for the linear time dependence (3) of the frequency $\omega(t) = (\omega_0 + \sigma \cdot t)$, the limitary velocity $v_1^* = l \cdot \sqrt{\pi \cdot \sigma}$ (9) is constant and the function $\theta(t)$ (14) has the form:

$$\theta(t) = 1 - exp\left[-0.564 \cdot \sqrt{\sigma} \cdot t\right]. \qquad (15)$$

It is important also to analyze the following average kinetic energy $K_a(t)$ of particles captured in the electromagnetic trap up to the moment t:

$$K_a(t) = \frac{0.5}{\theta(t)}\int_0^t E(t,t_1)\frac{\mathrm{d}\theta(t_1)}{\mathrm{d}t_1}\,\mathrm{d}t_1 \qquad (16)$$

In Eq.(16) the energy $E(t,t_1)$ is determined by the relationship (6) and under our conditions may be presented in the following form on the basis of the adiabatic invariant (7):

$$E(t,t_1) = \frac{m\cdot\omega(t)\cdot v_1^2}{2\omega(t_1)} + \frac{m\cdot\omega(t_1)\cdot\omega(t)\cdot l^2}{2} \approx \frac{m\cdot\omega(t_1)\cdot\omega(t)\cdot l^2}{2}, \qquad (17)$$

where we used the relationship $v_1^2 \ll \omega(t_1)^2 \cdot l^2$, which proceeds from the formula (9) at the adiabatic change of the frequency $\omega(t)$ (4). According to eqs. (16) and (17), the initial average energy of trapped particles $E_a(t) \to 0.5m \cdot [\omega(t=0)\cdot l]^2$ when $t \to 0$.

Fig.2 presents time dependences of the relative depth $[\omega(t)^2/\omega_0^2]$ of the potential well (1) and also the fraction $\theta(t)$ (15) and the average kinetic energy $K_a(t)$ (16) of particles captured in the trap at the linear growth of the frequency $\omega(t)$(3). We can see that about 97% of particles in the cell are trapped during the indicated period (Fig.2b), while the potential depth increases only on the factor 2.25 (Fig.2a). It is important, that in spite of growth approximately on the factor 1.7 during this time, the average kinetic energy $K_a(t)$ of given trapped particles still is much less that the mean kinetic energy $0.25\,m \cdot u^2$ of free particles without electromagnetic trap (Fig.2c). Such a "cooling" of trapped particles is caused by their inelastic collisions with cell walls, when their speeds may lower up to magnitudes available for following capture of these particles. The considered process may occur sufficiently quickly. For example, in Fig.2 the indicated time interval $2*10^4$ (l/u)~1s when the length of the one-dimensional cell $2l$~1 cm and the most probable speed of free particles u~10^2 m/s.

3. DISCUSSION OF RESULTS

Results of the previous section were obtained for the comparatively simple one-dimensional model of the gas cell and the definite potential well (1). Corresponding calculations are much more complicated for real two- and three-dimensional systems. However numerical calculations carried out by author for gas cells with cylindrical and spherical symmetry and various spatial dependences of increasing (in time) potential wells confirmed following qualitative results 1-4 obtained in the section 2.

1). Even a highly shallow but increasing with time potential well will continuously capture sufficiently slow-speed particles of a strongly rarefied gas in a cell.

2). Such trapped particles will remain in the potential well and will not collide with cell walls even after going out of the corresponding nondecreasing electromagnetic field on a stationary value.

3). These electromagnetic traps are especially effective in cases of inelastic collisions of still nontrapped particles with walls of the gas cell. Then necessary slowdown of given particles is possible for their following capture in the potential well. The accumulation process of comparatively slow-speed particles in the trap takes place during intensification of the electromagnetic field because a probability of such slowdown collisions increases with time.

4). At definite conditions, an average speed of particles captured in considered electromagnetic traps will be much less than the most probable speed of such free particles in the gas cell without given traps.

Of course, given results 1-4 are valid only in the absence of an interaction between particles in the gas cell. However such an interaction may be essential at a sufficiently high concentration of captured particles in a comparatively small volume of the trap.

We have considered new electromagnetic traps for structureless particles having an electric or magnetic moment. In practice such situations may take place, in particular, for a collection of micro- or nano-particles, which fly in a cell under conditions of the ultrahigh vacuum at action of the controllable nonhomogeneous electric (magnetic) field or nonresonance laser radiation.

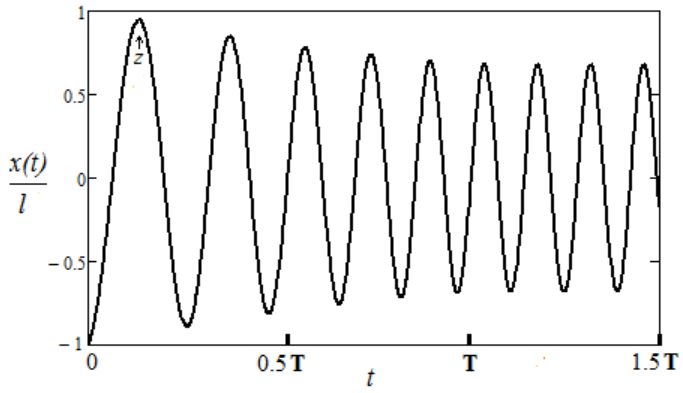

Fig.1. The one-dimensional motion of a particle, which is reflected with the velocity v_1 from the cell wall with the coordinate $x = -l$ in the moment t=0 in case of the time change of the frequency $\omega(t)$ according to the formula (3), when $v_1 = 5(l/T)$, $\omega_0 = 20/T$ and $\sigma = 25/T^2$.

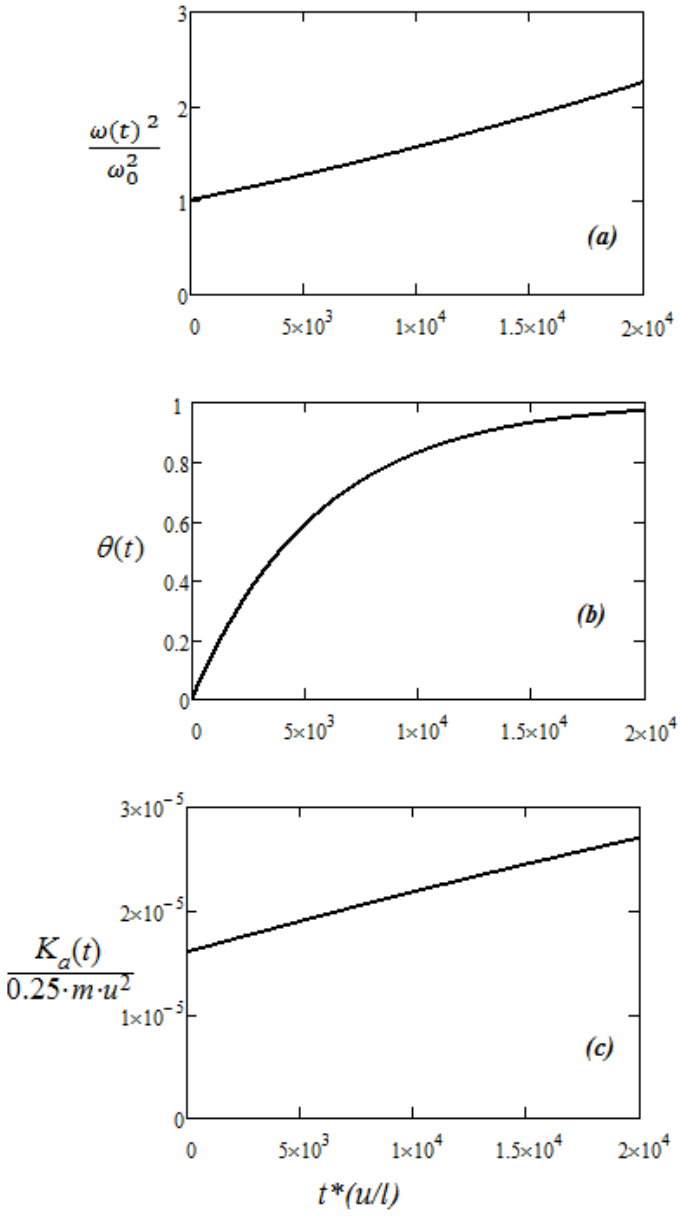

Fig.2. Time dependences of the relative potential depth~$[\omega(t)^2/\omega_0^2]$ (a), the fraction $\theta(t)$ (b) and the average kinetic energy $K_a(t)$ (c) of particles captured in the trap in case of the linear growth of the frequency $\omega(t) = \omega_0 + \sigma \cdot t$, when $\omega_0 = 4 \cdot 10^{-3}\ (u/l)$ and $\sigma = 4 \cdot 10^{-7}\ (u/l)^2$.

For analysis of possible capture of atoms and molecules in proposed traps, consideration of their quantum structure is necessary. Meanwhile, in definite cases, results obtained in this paper may be generalized also on such quantum objects. Thus, for example, it is possible creation of two- and three-dimensional traps for atoms and molecules by the nonhomogeneous laser radiation with frequencies essentially detuned from resonances with atomic (molecular) transitions [8-10]. Then the gradient force acts on atoms (molecules) in the direction to the point of minimum of the light induced potential well. However such a well is usually so shallow that a preliminary slowdown of particles up to very low speeds is necessary for their trapping. Unlike some atoms [1,8], such an effective "cooling" can not be realized for most molecules because of their complicated structure [9,10]. However it is possible to realize the necessary slowdown and following trapping of a large number of ground state molecules in a compact gas cell by the more universal method proposed in the present paper. Indeed, then an inelastic (in particular diffuse) reflection of nontrapped molecules from cell walls is necessary. A collection of captured molecules by the proposed method will have much less characteristic speed in comparison with free molecules in the absence of the electromagnetic trap. Thus, in particular, an essential decrease of Doppler widths of absorption (or fluorescence) spectral lines of trapped molecules in the gas cell may be recorded by the additional probe radiation.

---

[1] *Ashkin.* Optical Trapping and Manipulation of Neutral Particles Using Lasers. (World Scientific Publishing, 2006).

[2] *W. Demtroder.* Laser Spectroscopy: Basic Concepts and Instrumentation. (Springer, Berlin, 2003).

[3] *F. Riehle.* Frequency Standards-Basics and Applications. (Berlin: Wiley-VCH, 2004).

[4] *A.Ch. Izmailov.* "Trapping of classical particles by a potential well deepening with time", Azerb. Journal of Physics, 2015, V. **XXI**, N2, pp. 32-35.

[5] *A.Ch. Izmailov.* "Trapping of classical particles by an electromagnetic potential well deepening over time", Optics and Spectroscopy, 2015, V. **119**, N5, pp.883-886.

[6] *V.I. Arnol'd.* Mathematical Methods of Classical Mechanics. (Springer, 1989).

[7] *Ching Shen.* Rarefied gas dynamics: Fundamentals, Simulations and Micro Flows. (Springer, 2006).

[8] *H.J. Metcalf, P. Straten.* Laser cooling and trapping. (Springer, 1999).

[9] *L.D. Carr, D. DeMille, R.V. Krems, and Jun Ye.* "Cold and Ultracold molecules: Science, Technology and Applications", New Journal of Physics, 2009, V.**11**, 055049.

[10] *M. Lemeshko, R.V. Krems, J.M. Doyle, and S. Kais.* "Manipulation of molecules with electromagnetic fields", Molecular Physics: An International Journal at the Interface Between Chemistry and Physics, 2013, V. **111**, N12-13, pp.1648-1682.

Recevied: 07.04.2016

CONFORMATIONAL RECONSTRUCTIONS IN CREKA MOLECULE STRUCTURE IN MOLECULAR DYNAMICS PROCESS

G.J. ABBASOVA, E.Z. ALIYEV
Cafedra of optics and molecular physics
Baku State University

The spatial and electron structure of CREKA molecule which is new medicine possessing the antitumoral effect is investigated by molecular dynamics method. The geometric parameters and energy contributions of different types of interatomic interactions in stabilization of stable conformational molecule states are calculated, the quantitative evaluation of change limits of dihedral angles in main and side chains of amino-acid residuals in process of molecular dynamics is carried out.

Keywords: CREKA, peptide, conformational analysis, conformational state, molecular dynamics.
PACS: 31.15;33.15

INTRODUCTION

The more perspective directions in investigations of structure and properties of biological system on molecular and cell levels are connected with nanobiotechnology the aim of which is the control by the transport of medicinal and diagnostic agents. The loaded nanoparticle concentrates in itself the several decades of thousands and more molecules of medicinal agent that gives the possibility of effective transport of chemical compounds directly to the delivery place without affection of healthy cells of different organs and tissues.

The compound consisting of five amino-acid residuals Cys1-Arg2-Glu3-Lys4-Ala5 and called CREKA belongs to the number of such medicinal agents applied in tumor cell therapy using the nanoparticles. CREKA medicine possessing the strongly expressed anticancer effect in respect of prostate cancer had been firstly synthesized in 2006 by American scientists of Technical University of Massachusetts [1]. Further, its pharmacological properties had been studied [2-3]. The spatial structure and conformational properties of CREKA molecule are investigated in the given work by molecular mechanics method using the computer programs. The calculations are carried out by the method of theoretical conformational analysis by the technique which is given in detail in [4-5]. The conformational states of Arg2-Glu3, Cys1-Arg2-Glu3, Cys1-Arg2-Glu3-Lys4 fragments and further of whole CREKA molecule are gradually calculated on data based on mono-peptide molecules.

CALCULATION METHODS

The method of equilibrium molecular dynamics (MD) the progress, in development of which is based on achievements of computer technologies [6], is widely used under different conditions for description of dynamic behavior of peptide molecules. MD calculations are carried out in conditions of implicitly given water molecules with taking into consideration of (ε) medium dielectric constant. It is known that dielectric constant change influences on balance of electrostatic interactions of functional groups of amino-acid residuals in peptide molecules and essentially influences on hydrogen bond formation and its number. In all cases the calculated equilibrium geometry is used as the initial one for molecular-dynamic calculation carried out in potentials of semiemperical method MM+ without taking into consideration the symmetry. The optimization of molecule geometry is carried out with convergence parameter 0.01.

THE RESULTS AND THEIR DISCUSSION

The molecular dynamics of peptide in conditions modeling the implicitly water surrounding is studied for revealing of conformational stable and relatively labile parts of CREKA molecule. The collisional thermostat towards Berendsen one is used for keeping of temperature constancy. The time constant of velocity change in Berendsen thermostat is equal to τ=0,5. The periodic boundary conditions with cubic cell 100x100x100 Å are used. The cutoff radiuses are: a) for electrostatic interactions 21 Å; b) for Van-der-Waals interactions 16,8Å. It is known that change of torsion angles φ and ψ make the contribution in polypeptide chain flexibility, that's why the change limits of dihedral angles in molecule main chain at molecular dynamics process are given in table 8. The dihedral angles (grad) in low-energy conformations of CREKA molecules before (headline) and after (bottom line) molecular dynamics in MM+ force field are shown in table 1.

As it follows from the calculation results the state with minimal energy value (conformation 1, fig.1) undergoes the conformational reconstructions because of ψ angles, moreover, almost similarly for all amino-acid residuals. The molecule gains the more extended structure, in which only side chains of Arg2 and Glu3 residuals with opposite charged functional groups are connivent ones. In conformation 2 the reconstructions are related to main chains of Glu3, Lys4 and Ala5 residuals, the result of which is the closeness of Ala5 and Lys4 side chains. The changes in arginine residual structure are connected with insignificant conformational reconstructions in its side chain. 3 and 4 conformations keep the structure compactness and closeness of end residuals in spite of change of main chain step due to the change of angle ψ in Arg2 from value -63^0 to $+63^0$ and angle φ in Glu3 from -96^0 to 72^0.

131 H.Javid ave, AZ-1143, Baku
ANAS, G.M.Abdullayev Institute of Physics
E-mail: jophphysics@gmail.com

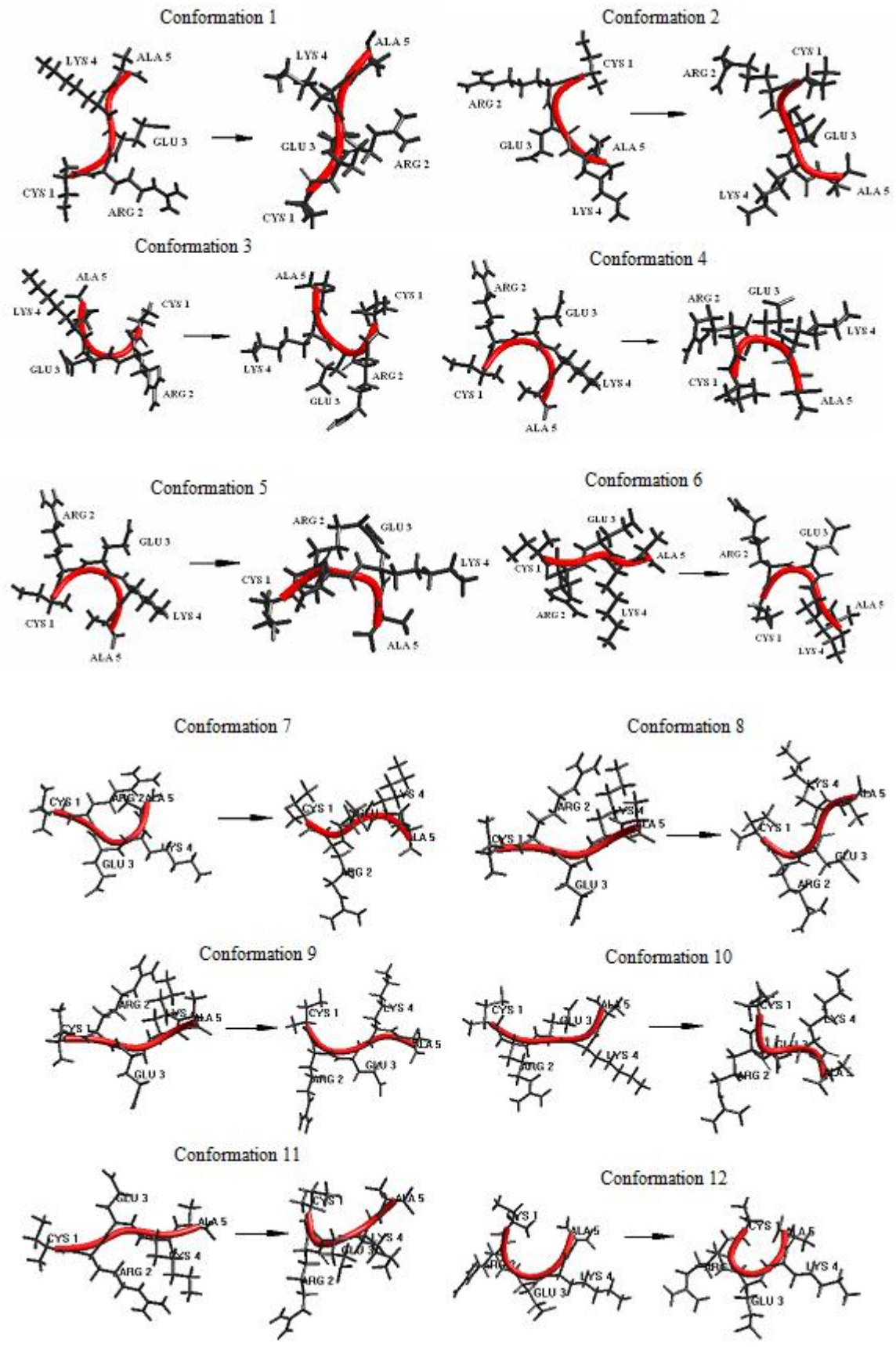

Fig.1. Conformational reconstructions in CREKA molecule structure.

Table 1.

The dihedral angles (grad) in low-energy conformations of CREKA molecules before (headline) and after (bottom line) molecular dynamics in MM+ force field

Conformation	Cys1	Arg2	Glu3	Lys4	Ala5
1	*-73, -55, 180 -145, -67, 182	-104, -59, 178 -96, 56, -172	-99, 137, 185 -82, 35, 164	-117, -61, 184 -99, 60, -171	-88, -52, 178 -58, 180, 179
2	-76, -52, 180 161, -164, 189	-92, -56, 178 -102, -28, -175	-147,173,180 -101,107,-168	-90, 95, 180 -67, 30, -175	-84, -55, 179 -119,172, 164
3	-83, 72, 181 -53, 93, 176	-116,-63,177 -96, 63, 169	-96,-52,183 72, -40, -172	-114,123,175 -83, 57, -161	-83,-54, 180 -42, 146,174
4	-83, 76, 181 -50, 93, 177	-119, -63, 179 -88, 31, 171	-94, 140, 187 80, -44, -165	54, 65, 184 -74, -52, 159	50, 56, 188 -88, 118, 169
5	-77,-57,179 -90, -73, 185	-108,-61,178 -86, 45, -176	-98,143,186 -73, 55, 178	55, 68, 181 87, -72, -166	-113, 141, 183 -162,-168,-173
6	-87, -62, 180 174, -176, 181	-136, -63, 180 -98, 70, -164	53, 62, 183 70, 12, 173	-117, 96, 182 -95, 68, 171	-89, -56, 180 -63, -38, 169
7	-88, -63, 180 -74,104,182	-137, -62, 180 -103,11,179	53, 68, 180 72,-18,-173	60, 68, 183 65,39,174	-111, 141, 177 -165,-85,-168
8	-89,-62,180 161,72,179	-138,-63,179 -73,59,-176	53,59,183 79,53,-178	-113,-61,182 -88,71,173	-86,-54,179 -101,99,-161
9	-82,85,181 81,82,186	-105,-62,179 69,-31,179	-98,139,188 -103,68,-179	-116,-60,181 -72,-57,173	-87,-52,178 -167,48,-177
10	-79,84,181 106,159,182	-103,101,181 -90,-23,-170	-107,167,189 -86,75,164	-83,-53,177 -156,-48,180	-83,-53,176 -160,-19,173
11	-79,83,181 170,73,188	-113,-62,180 -75,54,168	50,62,179 72,40,-180	-120,94,181 -84,82,-176	-89,-56,180 120,27,177
12	80,-58,180 53,-78,184	-113,-58,178 -71,-64,180	-104,-74,176 -118,-54,177	-128,-68,193 174,-47, 171	189,-51,189 -151,- 68,174

*Note: The values of dihedral angles of the main chain are given in consistency: φ, ψ, ω.

The essential reconstructions are revealed in molecular dynamics processes in 5 and 7 conformations in difference on the conformations above mentioned.

The changes in angle ψ in Arg2 from -61^0 to $+45^0$ and also changes of angle ψ in Lys4 from $+68^0$ to -72^0 lead to the formation of more disordered structure.

The hydrogen bond rupture between atoms of peptide group NH in Cys1 and COO in Glu3 takes place in conformations 6,8-11 because of formation of strong intramolecular interactions between atoms of side chain of Cys1 and Lys4 residuals.

The sum energy of such interactions is higher on 0,8 kcal/mol than formation energy of hydrogen bond.

The conformation 12 is more stable one in respect of main chain angles. The insignificant changes in Arg2 main chain leads to formation of more compact structure with connivent final sections.

The interatomic spacing between C^{α}-atoms of Cys1 and Ala5 residuals decreases from 6.4 up to 4.2 Å.

CONCLUSION

Thus, summarizing the investigation results one can conclude the following: in spite of the data of molecular mechanics method the conformation 12 is less on 3,4 kcal/mol than other low-energy conformational states.

It is more stable one in respect of intramolecular interactions in molecular dynamics process.

This allows us to conclude that especially this conformational state of CREKA molecule is the more stable one to surrounding action and can keep the spatial structure elements to realize its biological functions.

The obtained results will be used for molecular modeling of CREKA molecule analogues and study of their structural-functional interaction with the aim of revealing of common elements of spatial structure which are responsible for pharmacological effects of investigated compound. Such investigations can be the basis for further synthesis of new medicinal agents with controlling therapeutic effect.

[1] *O.C. Farokhzad, J.J. Cheng, B.A. Teply, I. Sherifi, S. Jon, P.W. Kantoff, J.P. Ritchie, R. Langer.* 2006. Targeted nanoparticles–aptamer bioconjugates for cancer chemotherapy in vivo. *Proc. Nat. Acad. Sci.* **103,** 6315-6320.

[2] *A. Fleischmann, U. Laderach, H. Friess, M.W. Buechler, J.C. Reubi.* 2000. Bombensin

receptors in distinct tissue compartments of human pancreatic diseases. *Laboratory Investigation*, **80**, 1807-1817.

[3] *X. Montet, R. Weissleder, L. Josephson.* 2006. Imaging pancreatic cancer with a peptide–nanoparticle conjugate targeted to normal pancreas. *Bioconjugate Chemistry*. **17**, 905-911.

[4] *P. Couvreur, C. Vauthier.* 2006. Nanotechnology: intelligent design to treat complex disease. *Pharm.Res*., **23** (7), 1417-1450.

[5] *Q.M. Lipkind, S.F. Arxipova, E.M. Popov.* 1970. Jurnal structurnoy ximii. **11**, 121-126. (In Russian).

[6] *K.B. Shaytan.* Molekulyarnaya dinamika peptidov. (In Russian).

[7] (www.moldyn.ru/bioinzhenerija/doc/stat/moldyn.htm)

Received: 14.03.2016

INSIGHTS INTO BIOACTIVE CONFORMATION OF DERMORPHIN

G.A. AKVERDIEVA
Institute for Physical Problems, Baku State University, Z.Khalilov st.23, AZ-1148, Baku, Azerbaijan

The conformational profiles of opioid peptide dermorphin and its active analog have been investigated within molecular mechanics framework and detailed by molecular dynamics simulations and quantum-chemical calculations. On the basis received results and data of SAR studies the bioactive conformation of dermorphin was assessed and the model of pharmacophore for the interaction of this molecule with the opioid receptors was proposed.

Keywords: dermorphin, conformational analysis, molecular dynamics, electronic structure, pharmacophore.
PACS: 36.20.Ey; 36.20.Fz; 36.20.Hb

1. INTRODUCTION

Dermorphin is linear peptide, isolated from a skin of the Southern-American frogs belonging to family Phyllomedusa, has high relationship and selectivity to μ-opioid binding places, but possess certain affinity to receptors δ- type [1-5]. Dermorphin shows strong analgetic influence as on central and peripheral nervous systems that is reflected in various physiological functions of an organism: cardiovascular, immune, anti-inflammatory, thermoregulatory and etc. This peptide is about 30-40 times more potent than morphine [6]. Dermorphin has been illegally used in horse racing as a performance-enhancing drug [7]. Many works are devoted to the structure-functional investigations of peptides of this family [8-12]. In this work using molecular modeling the comparative conformational analysis of dermorphin and its active tetrapeptide analog (1-4)dermorphin [11] was performed and the optimal conformations common to these molecules were found, on the basis received results and data of SAR studies the bioactive conformation of dermorphin was assessed and the model of pharmacophore for its interaction with the opioid receptors was proposed.

2. METHODS

Conformational energy calculations were made with an IBM computer using version of ECEPP (Empirical Conformational Energy Program for Peptides) written in FOTRAN [13,14]. The program was developed from the matrix method principle of Hermans and Ferro [15]. The investigations were carried out within molecular mechanics framework as described in [16,17]. The backbone was described by the "shape" symbols *e* and *f* corresponding to extended and folded configuration of virtual bonds C^{α}_{i}- C^{α}_{i+1}- C^{α}_{i+2}- C^{α}_{i+3}, respectively. The nomenclature and conventions adopted are those recommended by IUPAC-IUB [18].

The molecular dynamics of dermorphin was spent with use of force field AMBER in the temperature interval 293-313K with step 5K during 10 nanoseconds by means [19]. Procedure solvation with application of model of water in the set spherical volume TIP4P [20] has been used. The quantum- chemical calculations of these molecule were conducted by method CNDO [21], used the demonstration version of software package HyperChem (http:// www.hyper.com).

3. RESULTS AND DISCUSSION

3.1. Conformational profiles of dermorphin and (1-4)dermorphin

In first step the conformational possibilities of (1-4) dermorphin have been investigated on the basis of low-energy states of monopeptides. It is establishment, that the conformations of 8 shapes of backbone fall within the 0 - 5 kcal/mol interval. The energy parameters of these conformations are listed in Table1.

As may be inferred from these data, the structures of tetrapeptide with the folded backbone shapes of the N-terminal dipeptide part are the most preferred ones and correspond to stabile states of this sequence. They are representatives of *fee, ffe, fff, fef*-shapes with relative energies in within 0-2 kcal/mol. The mono- and dipeptide interactions are more effective in these structures. The nonvalent interactions of the side chains of Tyr and Phe residues are the major contribution to the conformational energy of this peptide. These interactions are most fully realized in the conformations of mentioned four shapes. Global conformation $L_{21}LB_{11}R$ of this sequense belongs to *fee* shape. This conformation is more favorable among preferred structures on nonvalent interactions. In addition, in this conformation the most successful compromise between the electrostatic and torsion interactions is achieved. Second structure $L_{21}PB_{11}R$ has *ffe* shape of backbone. There is a strong tripeptide interaction between the amino acid residues Tyr1 and Phe3 (approximately -5.7 kcal/mol) is realised in this structure. The effective tetrapeptide contributions (-4.7 kcal/mol) are characteristic for $B_{21}PB_{31}L$ conformation with spiral structure of backbone. The electrostatic interactions play an important role in its stabilization. The distance between the ends of the molecule is equal to 3.9 Å in this structure. Note that all structures of *fff* -shape are compact due folded forms of the main chain of residues. The relative energy of the other four shapes, namely, *eff, efe, eee, eff* changes in the interval 2-5 kcal/mol. The conformations of these shapes are losing in energy as the non-bonded and dispersion interactions, they are favorable only by torsion contributions. Although the form of the main chain of shapes *eee, eef* promotes the spatial separations of the of ends of this fragment (~ 12.5 Å), the rings of the residues Tyr and Phe are close together in space (3,4 Å) there. Table 2 shows the geometrical parameters of the preferred conformations of all shapes of peptide backbone of (1-4) dermorphin.

131 H.Javid ave, AZ-1143, Baku
ANAS, G.M.Abdullayev Institute of Physics
E-mail: jophphysics@gmail.com

Table 1. Energies of the favorable conformations of (1-4) dermorphin

Number	Shape	Backbone form	Energies of interactions										
			$\sum E_{inter.}$	Tyr1 DAla2	DAla2 Phe3	Phe3 Gly4	Tyr1 Phe3	DAla2 Gly4	Tyr1 Gly4	$E_{tot.}$	$E_{el.}$	$E_{conf.}$	$E_{rel.}$
1	*fee*	LLBR	2.6	-2.9	-1.9	-2.6	-3.1	-0.2	-0.5	-12.5	3.9	1.8	0
2	*ffe*	LPBR	4.1	-2.0	-1.0	-2.7	-5.7	-0.2	-1.6	-11.4	2.4	3.0	0.7
3	*fff*	BPBL	3.4	-3.2	-1.9	-0.6	-2.6	-0.5	-4.7	-12.2	2.3	3.9	0.7
4	*fef*	LLBL	2.5	-3.0	-1.9	-1.2	-3.2	-0.3	-0.4	-7.2	4.1	2.4	1.0
5	*eff*	RPRR	6.2	-2.6	-2.2	0.0	-3.5	-0.4	-3.2	-10.1	4.4	1.3	2.3
6	*efe*	RPBR	6.3	-2.3	-0.9	-1.8	-3.5	-0.2	-2.6	-9.4	4.3	1.8	3.4
7	*eee*	RLBR	5.8	-2.1	-1.3	-2.0	-3.4	-0.3	-0.5	-8.4	4.7	0.8	3.8
8	*eef*	RLBL	5.8	-2.1	-1.3	-1.1	-3.4	-0.4	-0.5	-7.6	4.7	0.8	4.7

Table 2. Geometry parameters (in degrees) of the favorable conformations of (1-4) dermorphin

Residue	Dihedral angles	Conformation							
		$E_{rel.}$=0.0 xcal/mol	$E_{rel.}$=0.7 xcal/mol	$E_{rel.}$=0.7 xcal/mol	$E_{rel.}$=1.0 xcal/mol	$E_{rel.}$=2.3 xcal/mol	$E_{rel.}$=3.4 xcal/mol	$E_{rel.}$=3.8 xcal/mol	$E_{rel.}$=4.7 xcal/mol
Tyr	φ	58	63	-72	58	-110	-110	-114	-113
	χ_1	177	179	177	178	179	176	181	-179
	χ_2	78	78	83	75	87	86	91	91
	χ_3	180	180	180	180	180	179	180	180
	Ψ	140	124	149	143	-64	-69	-59	-59
	ω	178	-172	-175	180	175	171	178	178
D-Ala	φ	95	78	77	94	80	73	101	101
	χ_1	180	178	179	-179	180	180	-179	-179
	Ψ	54	-60	-66	52	-80	-80	65	66
	ω	-179	170	166	180	-179	175	175	175
Phe	φ	-145	-107	-129	-144	-143	-119	-111	-111
	χ_1	60	66	-59	55	-60	60	63	62
	χ_2	94	89	88	90	90	90	88	88
	Ψ	168	170	130	161	-61	160	162	160
	ω	177	180	190	179	180	179	179	179
Gly	φ	-78	-77	71	83	-91	-91	-89	89
	Ψ	-72	-79	76	72	-90	-90	88	88
	ω	180	180	180	180	180	180	180	180

Table 3. Low-energy conformations of dermorphin

Number	Shape	Backbone form	$E_{tot.}$	$E_{el.}$	$E_{conf.}$	$E_{rel.}$
1	*fffffef*	LPBLLRR	-24.6	1.3	4.2	0
2	*feefee*	LLBRBBR	-24.5	3.1	2.7	0.4
3	*feefef*	LLBRBRR	-24.2	3.2	2.4	0.5
4	*fffffee*	LPRRBBR	-23.8	2.4	3.0	0.7
5	*feeeef*	BLBRBRR	-23.7	3.2	2.3	0.9
6	*efffef*	RPRRBRR	-24.0	3.8	2.2	1.0
7	*fefeee*	LLBLBBR	-24.1	3.0	3.1	1.1
8	*efffee*	RPRRBBR	-24.3	3.9	2.6	1.2
9	*ffefef*	LPBRBRR	-23.1	1.8	3.4	1.3
10	*fffeee*	BPBLBBR	-23.7	1.5	4.5	1.4
11	*ffefee*	LPBRBBR	-22.8	1.5	4.0	1.7
12	*feffef*	LLRRBRR	-23.8	3.6	2.8	1.7

*The energy parameters are given in kcal/mol

Table 4. Geometry parameters (in degrees) of the optimal conformations of dermorphin*

Residue	Conformation				
	$E_{rel.}$=0.0 xcal/mol	$E_{rel.}$=0.4 xcal/mol	$E_{rel.}$=0.5 xcal/mol	$E_{rel.}$=0.7 xcal/mol	$E_{rel.}$=0.9 xcal/mol
Tyr1	66, 179, 80, 180, 128,-173	58, 177, 78, 180, 141, 179,	58, 177, 78, 180, 141,179,	58, 180, 75, 180, 112, 180	-73, 63, 87, 180, 164, 178
DAla2	76, 178, -64, 167	95, 179, 54, -179	95, 179, 54, -179	80, 179, -70, 178	82, 179, 48, 179
Phe3	-114, 63, 86, 162, 175	-146, 59, 94, 169, 179	-146, 59, 94, 167, 177	-138, -61, 90, -63, -178	-142, 61, 87, 168, 179
Gly4	73, 76, 178	-77, -71, -179	-79, -72, 180	-96, -96, -178	-80, -76, 180
Tyr5	51, -172, 71, 180, 71, -178	-132, 65, 91, 180, 151, 173	-117, 55, 83, 180, 142, 174	-134, 64, 91, 180, 155, 175	-115, 54, 83, 180, 142, 175
Pro6	-62, -178	99, -177	-66, -175	100, -177	-67, -175
Ser7	-107, -60, 180, -61, -179	-97, 54, 180, -53, 180	-115, -60, 180, -60, 180	-97, 54, 180, -53, 180	-115, -60, 180, -59,180

*The values of dihedral angles are in the following order: φ, χ_1, χ_2, χ_3, Ψ, ω

In a further step the conformational analysis of dermorphin was carried out through a fragmental calculation on the basis of stable states of monopeptides. The starting structural variants for dermorphin yielded more than 400 conformations belonging to 32 shapes of peptide skeleton, 31 dihedral angles were exposed to

rotation. Despite rather limited conformational possibilities of the N-terminal part of this molecule, thanks to presence residue Gly in its sequence the effective interactions are realized between the terminal segments of molecule in the low-energy conformational states divided by a energy barrier, not exceeding 2 kcal/mol (See Table 3). The presence of proline residue in peptide sequence causes of the bend of peptide chain on the C-terminal tripeptide fragment and reduces the number of sterically allowed structural types for this part of molecule: the conformations only *ee* and *ef* shapes are possible for it.

The optimal conformations of dermorphin were assessed by pairwise cross comparisons of the low energy conformations found for dermorphin and (1-4) dermorphin. These results were compared also with data of two other tetrapeptide analogs of dermorphin - ARPG (H-Tyr-D-Arg-Phe-Gly-OH) and TDAPA (H-Tyr-D-Arg-Phe-beta-Ala-OH), which were studied previously [22,23]. It was found the optimal structures of dermorphin ($E_{rel.}$= 0.0 kcal/mol, 0.4 kcal/mol, 0.5 kcal/mol, 0.7 kcal/mol and 0.9 kcal/mol) are the folded or semifolded conformations stabilized by hydrogen bonds between the atoms of peptide skeleton. These results well coordinate to the data of spectroscopic works and theoretical researches [24-31], that offer as the preferable the semifolded or the folded forms of peptide skeleton of dermorphin molecule. The geometry parameters, the matrix of energy interactions and parameters of hydrogen bonds in the optimal structures of dermorphin molecule are listed in Tables 4, 5 and 6, respectively. These structures are shown in fig.1.

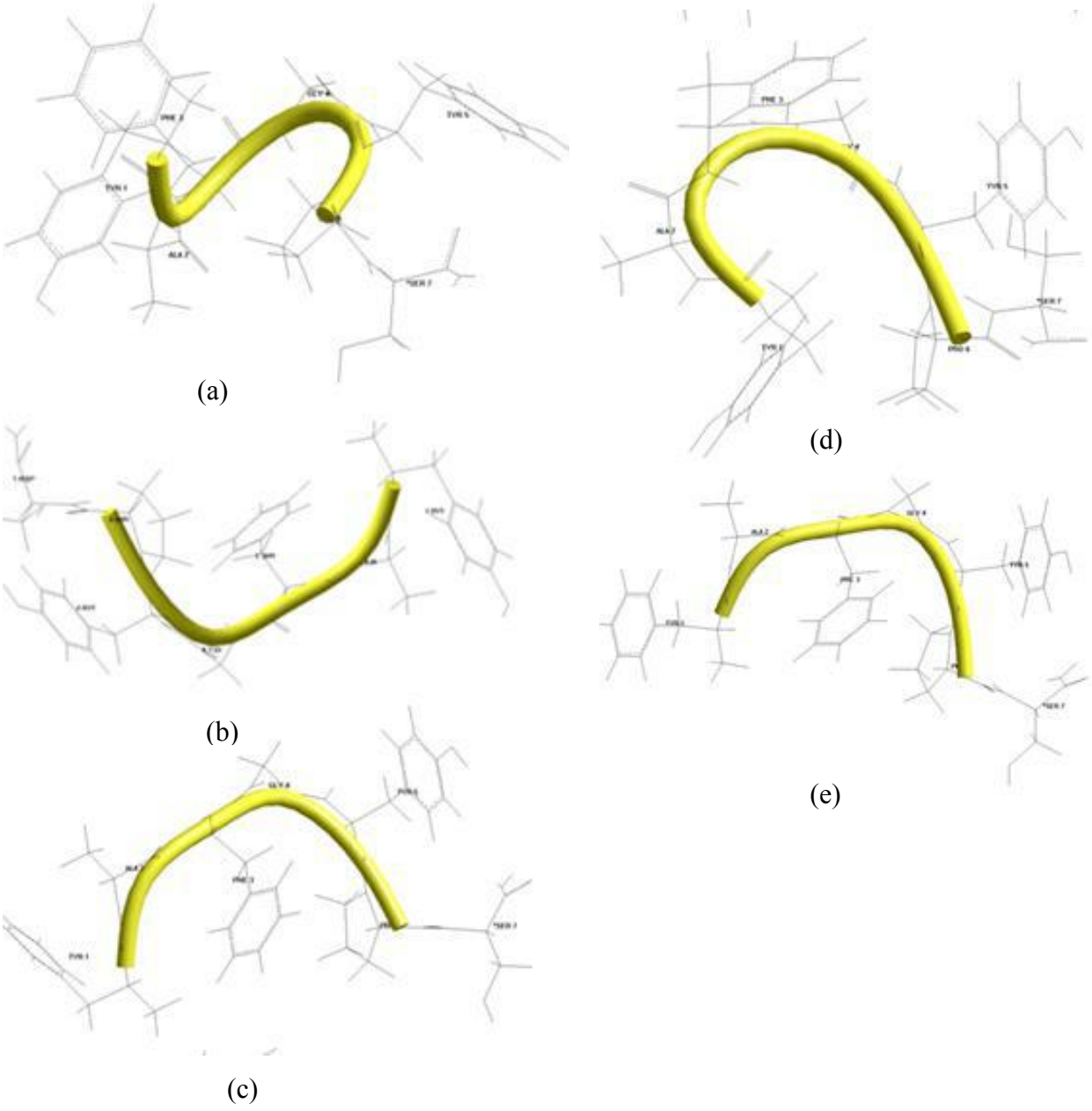

Fig.1. Optimal conformations of dermorphin with $E_{rel.}$= 0.0 kcal/mol (a), $E_{rel.}$= 0.4 kcal/mol (b), $E_{rel.}$= 0.5 kcal/mol (c), $E_{rel.}$= 0.7 kcal/mol (d), $E_{rel.}$= 0.9 kcal/mol (e)

Table 6. Inter- and intra-residue hydrogen bond lengths (in Å) and energies in brackets (in kcal/mol) in the optimal conformations of dermorphin[a]

H-bond	Conformation				
	$E_{rel.}$=0.0 kcal/mol	$E_{rel.}$=0.4 kcal/mol	$E_{rel.}$=0.5 kcal/mol	$E_{rel.}$=0.7 kcal/mol	$E_{rel.}$=0.9 kcal/mol
(Tyr1)NH...OC(Tyr1)	2.69 (-0.20)	2.54 (-0.30)	2.54 (-0.30)	2.74 (-0.17)	2.89 (-0.11)
(Tyr1)NH...OC(Tyr1)					2.40 (-0.46)
(Phe3)NH...OC(Phe3)	2.65 (-0.23)	2.33 (-0.56)	2.33 (-0.56)		2.36 (-0.51)
(Tyr5)NH...OC(Tyr5)		2.49 (-0.35)	2.67 (-0.21)	2.47 (-0.38)	2.69 (-0.20)
(Ser7)NH...O (Ser7)		2.46(-0.38)		2.46 (-0.38)	
(Tyr1)NH...OC(Phe3)	2.10 (-0.98)				
(Tyr1)CO...HN(Phe3)	2.00 (-1.20)			2.01 (-1.18)	
(Phe3)CO...NH (Tyr5)		2.51(-0.23)	2.55(-0.34)		2.52(-0.35)
(Tyr1)NH...OC(Gly4)				2.50 (-0.34)	
(Tyr5)CO...HN(Ser7)		2.49 (-0.35)		2.68 (-0.21)	
(Ser7)CO...H2N	2.52 (-0.33)	2.52 (-0.33)	2.52 (-0.33)	2.52 (-0.33)	2.52 (-0.33)
(Ser7)CO...H2N		2.52 (-0.33)	2.52 (-0.33)	2.52 (-0.33)	

[a] H-bond lengths are given without parentheses and corresponding H-bond energies are given in parentheses

Table 7. Characteristics of electronic structure of the optimal conformations of dermorphin

Conformation	$E_{rel.}$=0.0 kcal/mol	$E_{rel.}$=0.4 kcal/mol	$E_{rel.}$=0.5 kcal/mol	$E_{rel.}$=0.7 kcal/mol	$E_{rel.}$=0.9 kcal/mol
Dipol moment (D)	17.895	5.971	16.160	4.826	17.184
Total energy (kcal/mol)	-373340.976	-375078.471	-374842.040	-368144.928	-376271.080
Binding energy (kcal/mol)	-29080.191	-30817.686	-30581.254	-23884.143	-32010.295
Izolation atomic energy (kcal/mol)	-344260.786	-344260.785	-344260.785	-344260.785	-344260.785
Electron energy (kcal/mol)	-3349486.325	-3230127.022	-3210814.623	-3388005.513	-3179314.148
Energy of nuclear interaction(kcal/mol)	2976145.349	2855048.550	2835972.583	3019860.584	2803043.068
Energy of formation (kcal/mol)	-18087.799	-19825.294	-19588.862	-12891.751	-21017.903
E_{HOMO}	-9.252524	-8.109617	-10.558869	-9.044190	-10.916412
E_{LUMO}	0.991924	0.735477	0.732555	0.297698	1.948923
$\Delta E = E_{HOMO} - E_{LUMO}$	10.24	8.85	11.29	9.34	12.87

Table 8. The respective geometrical arrangement of pharmacophore elements of dermorphin

Distances	In Å	Angles	In degrees	Dihedral angles	In degrees
R_{12}	7.8	α_{121}	6.1	β_{2211}	-101.3
R_{13}	5.9	α_{131}	7.5	β_{3211}	50.4
R_{16}	6.2	α_{161}	9.3	β_{6611}	-140.3
R_{15}	8.4	α_{151}	4.9	β_{5511}	-136.3
R_{23}	2.4	α_{232}	10.2	β_{3322}	180.0
R_{26}	10.4	α_{262}	2.9	β_{6622}	-134.8
R_{25}	13.6	α_{252}	4.0	β_{5522}	-7.5
R_{36}	8.2	α_{363}	7.6	β_{6633}	64.0
R_{35}	12.9	α_{353}	5.0	β_{5533}	143.5
R_{45}	13.7	α_{454}	5.4	B_{5544}	-79.4

The physiologically active N-terminal tetrapeptid of dermorphin which defines the specificity of its interactions with opiate receptor has regular structure - α-spiral in two optimal conformations and semifolded structure in others optimal structures of dermorphin. As in this segment of the molecule the majority of the residues have folded backbone structure, the interactions of Tyr1 residue with the subsequent residues Ala2 and Phe3 by the contributions from -1.9 to -2.9 kcal/mol and from -2.2 to -5.2 kcal/mol, respectively and also the interactions of Tyr5 residue with the subsequent residues Pro6 and Ser7 by the contributions from -3.7 to -4.7 kcal/mol and from -2.9 to -3.8 kcal/mol, respectively, are effective. In the global conformation, belonging to *ffffef* shape of peptide skeleton, the residues Tyr1 and Phe3 with the aromatic side chains approach in space and form quasicyclic

structure with formation of two hydrogen bonds between amino and carboxyl groups of these residues. Therefore in this conformation the interactions of mentioned residues are stronger, than in other structures of molecule. This structure is characterized also by more effective contribution of interactions of residues D-Ala2 and Pro6 (-2.1 kcal/mol). In the conformations 2, 3 and 5 the dispersion contacts of residue Phe3 both with Tyr5 and with Pro6 are effective owing to their spatial approach and the interactions between atoms of aromatic side chains. These structures are characterized by existence of hydrogen bond (Phe3)CO…HN(Tyr5). For conformation 2 the hydrogen bond between the atoms of the main chain of the residues in fifth and seventh positions, namely (Tyr5)CO... HN(Ser7) is characteristic too, but thus HN group of Ser7 participates also in formation of hydrogen bond with O atom of own side chain. Conformation 4 (*fffffee*-shape) represents the particular interest. In this conformation the form of peptide chain of the N-terminal tetrapeptide part is similar to global conformations and the form of peptide chain of C -terminal tripeptide part is similar to conformation 2. Therefore the hydrogen bonds, characteristic for both specified conformations are realized in this structure. But distinctive features of conformation 4 are effective tetrapeptide interaction and formation of hydrogen bond (Tyr1)NH...OC(Gly4). As seen from the results, this conformation is distinguished from others by saturation of hydrogen bonds. In this structure the phenolic ring of the residue Tyr1 hangs over a conformationally rigid ring of the proline residue in the parallel position to it, and as result the interaction between these residues is found to be -4.1 kcal/mol. Here, α-amino group and the carbonyl residue Tyr5 are spatially close together, forming the salt bridge. The interactions of residue Tyr1 with Gly4 (-2.3 kcal/mol) and also with Tyr5 (-2.8 kcal/mol) bring the appreciable contributions to stabilization of this structure. Conformation 5 (*feeeef*-shape) is characterized by folded form of the N- and C-terminal dipeptide parts and by completely extended form of central part of the molecule. For this structure the intraresidual hydrogen bonds for residues Tyr1, Phe3, Tyr5 and also hydrogen bond between carboxyl group of main chain of Ser7 and H-atoms of the terminal amid group NH_2 are characteristic. All optimal structures of dermorphin are characterized by folded of conformation of the dipeptide segment Tyr1-DAla2 that is reason of strong dipeptide interaction. Apparently, the specified minimum structural requirement is important for physiological activity of dermorphin molecule, as it is necessary for protection of this peptide bond from splitting action by enzymes in the process of metabolism of peptide. Though, the specified spatial structures of this molecule are favourable as by energy and by entropic factors, the conformational changes with overcoming of a small energy barrier leading to realization of structures with the extended form of the N-terminal dipeptide segment are possible. Let's notice that structures 1, 9, 11 with L form of the main chain of Tyr1 can be realized also for its B form, slightly conceding in energy, accordingly, on 1.0, 0.7, 0.3 kcal/mol, as these forms of residue in first position differ in angle φ that determines the spatial arrangement of three identical hydrogen atoms with respect to the rest part of molecule. Apparently, from the Table 4, thanks to presence DAla and Pro in peptide chain a number of preferable structures have turns on the terminal parts of molecule. The particular interest is represented by the structures belonging *feefee* and *feefef* shapes of peptide skeleton with the relative energy, equal 0.4 and 0.5 kcal/mol. In these conformations β - turn is formed on the Gly4-Pro5 segment, therefore in them the aromatic side chain of residue Phe effectively interacts with atoms of the subsequent residues and the residue is shaden from solvent. amid proton of Gly4.

It was found that despite the conformational features of investigated optimal structures of dermorphin an α - amino group and the side chains of the tyrosine and phenylalanine residues are in the identical positions in space from each other in all of them. Dermorphin molecule forms compact structures, in which the residues Tyr1 and Ser7 point away from the core surface of molecule, that explains abilities of its OH-groups to interact with the environment. As these residues are capable to participate also in effective interresidual interactions, it is possible to assume that they should possess defined conformational dynamics.

3.2. Dynamic properties of dermorphin

Within the framework of mechanical model, a conformational dynamics of the side chains of the amino acid residues of dermorphin peptide was investigated. For this purpose, a series of conformational maps, or sections of the potential surfaces were constructed over the $\varphi - \chi_1$, $\chi_1 - \chi_2$, $\chi_2 - \chi_3$ or $\chi_1 - \chi_3$ angles for amino acid residues of the molecule [32]. Thus, the dihedral angles around the $N\text{-}C^{\alpha}$, $C^{\alpha}\text{-}C^{\beta}$, $C^{\beta}\text{-}C^{\gamma}$, $C^{\gamma}\text{-}C^{\delta}$ bonds of the side chains were varied, and the backbone of the peptide residues was fixed in accordance with the coordinates of the atoms of optimal structures of the peptide molecule. It has been found that Tyr1 has a considerable conformational mobility. The optimal positions of the Tyr1 side chain are close to the minima of their torsional potential : $\chi_1 = 60^0$, 180^0 , -60^0 and the deviations by $\pm 30^0$ from this values are possible. For χ_2 of the Tyr1 the changes by 30^0 from the values of the torsional minima $\pm 90^0$ are permissible. The angle χ_3 of Tyr1 can take values 0 and 180^0. This fact allows to conclude that such mobiliity of the tyrozin imidozol ring is probably necessary for the complementary binding with specific receptors. This result is very interesting because it correlates with the data from [33]. The investigation of φ-χ_1 conformational map of D-Ala2 revealed the permissible deviation by $+30^0$ from the optimal values of the φ angle. The optimal positions of the Ala1 side chain are close to the minima of their torsional potential: $\chi_1 = 60^0$, 180^0, -60^0 and the deviations by $\pm 30^0$ from these values are possible. The analysis of φ-χ_1 conformational map of Phe3 shows that the mobility of the φ angle is restricted. This angle can take a very fixed position and its variation leads to increase of energy in the whole molecule. Apparently, this fact can be explained due to the important role of this residue in formation of regular structure and of active form of molecule. Despite this, the angle χ_1 which orients the phenolic ring of this residue is mobile. The possible deviations of χ_1 for Phe3 from its torsion minima values 180 and -60^0 by $\pm 30^0$ and from value 60^0 by 30^0 are

allowed. The changes 15^0 are permissible for φ angle of Gly. The side chain of residue Gly4 consists of a single atom, so we can say that it is absent. For the angle φ of these residue the low-energy changes by 15^0 are admissible. Because of the amino acid residue Tyr5 precedes prolin and is located on a bend of the peptide chain conformational mobility of its φ angle is limited. Only minor changes, by 5^0 from optimal value of this angle are possible. The implementation of the positions of the side chain corresponding to the values 180 and -60^0 of χ_1 angle for this residue is possible. The deviations of χ_2 for Tyr5 by $+30^0$ from its optimal values $\pm 90^0$ are allowed. Calculated results indicate that χ_3 for Tyr5 can take two values, 0 and 180^0, corresponding to its stabile states. The deviations of χ_3 angle from these values lead to increase of energy in the whole molecule. Proline residue in the sixth position of the amino acid sequence is a specific residue. Its side chain is rigidly connected with the main chain and forms a cyclic structure. For this reason, the conformational mobility of this residue is impossible. The C-terminal residue Ser7 has large conformational dynamics. This residue is very mobile not only by side chain angles, but also by the φ angle of peptide chain. The changes by 50^0 are permissible for φ angle. The optimal positions of the Ser7 side chain are close to the minima of their torsional potential: $\chi_1 = 60^0$, 180^0, -60^0 and the low-energy barrier corresponding to the conformational transits between them equal 1.9 kcal/mol. The deviations of χ_2 of Ser7 by $+60^0$ from its optimal value are allowed.

Thus, the analysis of the conformational maps has revealed the degree of mobility of the functional residues. It is established that the dynamics of Phe3 and Tyr5 is limited owing to realization of effective stabilizing interactions of its aromatic side chains atoms with atoms of other residues of the molecule. So, the conformational freedom of Phe3 residue is limited by effective interactions with Tyr1, and conformational freedom of Tyr5 residue is limited by effective interaction of its aromatic ring with the atoms of the rigidly fixed prolin residue in sixth position. For this reason the conformational energy is rather sensitive to orientation of the side chains of specified amino acid residues. The side chains of Tyr1 and Ser7 are characterized by the large conformational dynamics. Evidently, such mobility of the terminal residues is necessary for realization of interactions with atoms of environment or receptor. As seen from the presented data, the conformational dynamics of any segment of a molecule is defined by efficiency of its interaction with other segments of molecule. The rotary possibilities of side chains of the residues are various among the considered optimal structures dermorphin, but because of presence of the hydrogen bonds the conformational balance is between them.

At the subsequent investigation step molecular dynamics of dermorphin has been studied and the most probable conformational states of this molecule are defined in vicinities of local minima at physiological temperature. As a result of simulation process, the ranges of change of dihedral angles and distances between atoms of amino acid residues are defined. The quantitative estimation of distances between atoms shows that at modeling the dispersion contacts between the amino acid residues in the first and fourth positions of peptide chain are invariable. The N-terminal tetrapeptide fragment of the molecule preserves the folded structure throughout molecular dynamics simulation, the distance between C^{α}- atoms of the specified residues does not exceed 7Å during simulation. The structure of this part of molecule upon termination of modeling process practically does not differ from the initial stage. It is possible to assume the conformational stability of specified fragment plays important role in functional activity of dermorphin molecule and defines the specificity of its interaction with the receptor. Because of mobility of the C-terminal tripeptide fragment of investigated molecule the distance between the atoms of the side chains of the residues Phe3 and Tyr5 is approximated to 2.8 Å during simulation. As result, the hydrogen bond between atoms of hydroxyl group of residue Tyr5 and the main chain of residue Phe3 is formed. Such conformational behavior may be due presence glycine in fourth position of peptide chain that is characterized by conformational freedom of rotation around C^{α}-$C^{/}$ and $C^{/}$-N bonds, giving certain flexibility to peptide chain. One can conclude, as the system is in an equilibrium state, the possible conformational changes are reversible. The cited data though testifies about stability of optimal conformations of dermorphin, but assumes also the probability of realizations of each of them depending on polarity of environment.

3.3. Electronic structure of dermorphin

As research of the electronic-conformational properties of biologically active molecules can be a basis for additional correlation of the spatial structure and structure-functional relationships, it is interesting to investigate the electronic structure of optimal structures of dermorphin. By optimization of electronic energy as zero states the equilibrium configurations of nuclease corresponding to geometry of the optimal structures of dermorphin have been considered. The half-electron approximation was used. The important parameters characterizing the electronic structure of the molecule have been calculated: the distribution of electronic density, the partial charges on the atoms, molecular orbitales, electric dipole moment, and also a number of energy parameters, such as the total energy, energy of the bind, isolated atomic energy, electronic energy, energy of nuclear interactions, heat of formation, highest occupied and lowest unoccupied molecular orbital energies that provide the information on stability of a molecule (see Table 7). It was established, that the optimal conformations 1-5 of dermorphin has low values of dipole moment and of energy $E_{HOMO,}$ characterizing its electro-donor properties and the energy of activation. It is possible to draw a conclusion that the low-energy structures of dermorphin have the insignificant chemical reactionary ability and the weak electrodonor properties. Apparently from the Table 7, the conformational distinction is reflected first of all in their electronic energy and energy of nuclear interactions. The structure 5 is characterized by folded forms of N- and C- terminal dipeptide sequences, it has lower values of bind energy, core-core interactions, heat of formation that is reflected in value of a total energy, but on value of dipole moment

it yields to structures 2-4. The structure 4, on the contrary, answers the low value of dipole moment (4.826 D) that is connected with its conformational features: the maintenance of the α - spiral on the N-terminal pentapeptide part of the molecule leads to rapprochement of polar groups of atoms of a molecule, but the destabilizing effect of interaction of cores is stronger here, and as a result it considerably concedes to other structures on value of a total energy. The structure 2 is characterized by two β - turns peptide chain answers to the steadiest electronic state of dermorphin. This structure is characterized by small value of dipole moment (5.971D), as well as structure 4, only slightly conceding to it, on value of a total energy it is the following stable structure after structure 5. As we see, the structure 2 is the most compromise for the basic parameters of electronic structure. It was found the conformational transitions between optimal structures of dermorphin are resulted by fluctuations of density of a charge on certain groups of the atoms, not exceeding 18%. The distinctions of charges on the atoms C-terminal dipeptide residues and amid group are revealed.

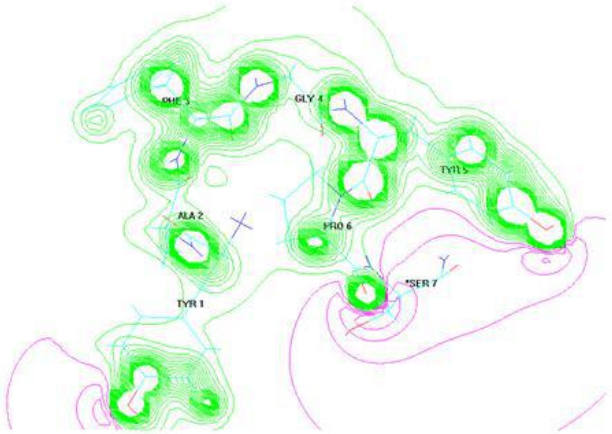

Fig.2. Two-dimensional contours of electrostatic potential in dermorphin molecule.

The distribution of charges on the atoms of the α - amino group and atoms of the side chains of tyrosine and phenylalanine residues are similar for optimal structures, that may be correlate with their biological activity - ability to participate in ligand-receptor interactions. Two-dimensional contour of electrostatic potential for this molecule is shown in fig.2. Green and violet colors represent, accordingly, positive and negative charged segments of the molecule. Apparently from the presented figure, there is the zone of high electronic density subjected to attack of the electrophil reagent.

3.4. Model of pharmacophore for the interaction of dermorphin with the opioid receptors

The review of the works [10-12, 26-27, 33-36] shows that the basic elements defining a way of interaction of opiate peptides with receptors are α - an amino group, the aromatic side chains of residues Tyr1, Phe3 and Tyr5. The spatial arrangement of the structural elements occupying the pharmacophore area and characterizing by specific electronic features may be the important criteria of the biologically active conformation of dermorphin. On the basis of the received results and data of SAR studies the bioactive conformation of dermorphin was assessed and the model of opioid pharmacophore for its interaction with opioid receptors was proposed (see fig.3).

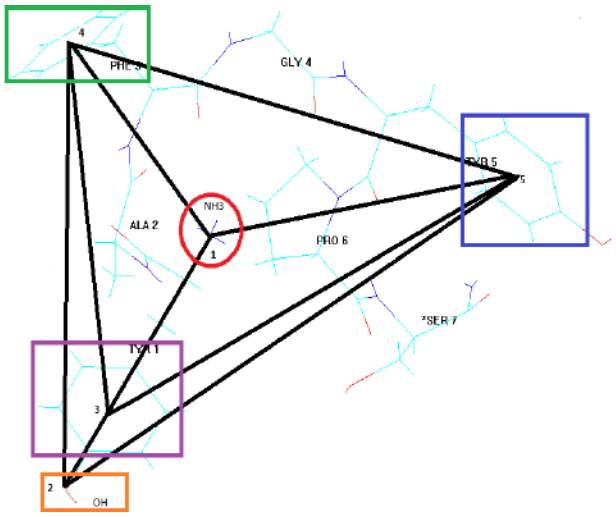

Fig.3. The model of proposed pharmacophore for the recognition of dermorphin to the opioid receptors.

The proposed model contains five areas which are occupied by pharmacophore elements marked by numbers 1-5. The pharmacophore element 1 represents the α - an amino group, namely, the protonated nitrogen atom participating in electrostatic interaction with negatively charged residue of opioid receptor. Thus there is also the formation of hydrogen bond with participation of protonated nitrogen atom. Such interaction in turn can lead to rupture of hydrogen bond between the transmembran spirals of opioid receptor AspIII:7... TyrVII:11 that leads to its activation [36]. The pharmacophore element 2 is presented by hydroxyl group of the side chain of residue Tyr1, it participates in the transit of a charge as the donor of electronic density and in the formation of the hydrogen bond. The pharmacophore elements 3 and 4 represent, accordingly, a phenolic ring of residue Tyr1 and an aromatic ring of residue Phe3, they participate in hydrophob interactions. The pharmacophore element 5 - a phenolic ring of the residue Tyr5 can participate in hydrophob interactions or in the formation of hydrogen bond, that defines the selectivity of this ligand. It should be noted that the pharmacophore elements 1 and 2 represent the affine areas, the pharmacophore elements 3 and 4 – the agonistic areas, the pharmacophore element 5 - antagonistic area of this pharmacophore. In represented model the centres of pharmacophore areas 1 and 2 were taken as protonated nitrogen atom and oxygen atom of hydroxyl group of the side chain of residue Tyr1, respectively; the centres of pharmacophor areas 3-5 were taken as the centres of weights of the structural fragments occupying the corresponding pharmacophore areas. The relative positions of pharmacophore areas of dermorphin molecule

are characterized by a set of distances, angles and dihedral angles (see Table 8):

1) the distances (R_{12}, R_{13}, R_{14}, R_{15}, R_{23}, R_{24}, R_{25}, R_{34}, R_{35}, R_{45}) between the centres of the specified pharmacophore areas;
2) the angles (α_{121}, α_{131}, α_{141}, α_{151}) " centre of pharmacophore area 1- centres of pharmacophore areas 2-5 – hydrogen atom in pharmacophore area 1";
3) the angles (α_{232}, α_{242}, α_{252}) "centre of pharmacophore area 2- centres of pharmacophore areas 3-5 – hydrogen atom in pharmacophore area 2" ;
4) the angles (α_{343}, α_{353}) "centre of pharmacophore area 3- centres of pharmacophore areas 4-5 – nearest atom to the centre of pharmacophore area 3";
5) the angle (α_{454}) "centre of pharmacophore area 4- centre of pharmacophore area 5 – nearest atom to the centre of pharmacophore area 4" ;
6) the dihedral angles (β_{2211}, β_{3311}, β_{4411}, β_{5511}) "centres of pharmacophore areas 2-5 –nearest atom to the centres of pharmacophore areas 2-5 - centre of pharmacophore area 1- hydrogen atom in pharmacophore area 1";
7) the dihedral angles (β_{3322}, β_{4422}, β_{5522}) "centres of pharmacophore areas 3-5 –nearest atom to the centres of pharmacophore areas 3-5 - centre of pharmacophore area 2- hydrogen atom in pharmacophore area 2";
8) the dihedral angles (β_{4433}, β_{5533}) "centres of pharmacophore areas 4-5 – nearest atom to the centres of pharmacophore areas 4-5 - centre of pharmacophore area 3 - nearest atom to the centre of pharmacophore area 3";
9) the dihedral angle β_{5544} "centre of pharmacophore area 5– nearest atom to the centre of pharmacophore area 5 - centre of pharmacophore area 4 - nearest atom to the pharmacophore area 4".

The proposed model defines the presence of the similar structural elements of the bioactive molecules participating in the interaction with opioid receptors. It is expected that received results can be used for search of the ligands of opioid receptors as pharmacological preparations with effective action.

4. CONCLUSION

Generalising results of research of the structure-functional relationship of dermorphin are next:

1. Optimal structures of a molecule dermorphin are characterized by folded conformation of the dipeptide segment Tyr1-DAla2. Apparently, the specified minimum structural requirement is necessary for protection of this peptide bond from splitting action by enzymes in the process of metabolism of peptide;
2. The physiologically active N-terminal tetrapeptide fragment of dermorphin has regular structure - α-spiral in two optimal conformations and semifolded structure in others. Conformational stability of this fragment, apparently, plays important role in functional activity of dermorphin molecule and defines the specificity of its interaction with the opiate receptors;
3. In two optimal structures of dermorphin β-turn is formed on the Gly4-Pro5 segment and the amid proton of Gly4 residue is shaden from solvent;
4. The structure characterizing by folded forms as of the N –terminal and the C-terminal dipeptide segments and by completely extended form of central part of molecule sequence is also answered to equilibrium state of dermorphin;
5. The conformational dynamics of Phe3 and Tyr5 is limited owing to realization of effective stabilizing interactions of its aromatic side chains atoms with the atoms of other residues of the molecule;
6. The residues Tyr1 and Ser7 are localized on a surface of molecule and characterized by large conformational dynamics;
7. The distribution of charges on the atoms of pharmacophore elements in the optimal structures are similar that confirms their identical arrangement in space from each other in all of them and may be correlated with their ability to participate in ligand-receptor interactions;
8. On the basis of the received results and SAR studies the bioactive conformation of dermorphin was assessed and the model of pharmacophore for interaction of this molecule with the opioid receptors was proposed;

The represented results are helpful for the study of the biology active forms of opioid peptides and for the design of opioid peptiomimetics.

[1] *P.C. Montecucchi, R. De Castiglione, S. Piani, L. Gozzini, V. Erspamer*, Amino acid composition and sequence of dermorphin, a novel opiate-like peptide from the skin of Phyllomedusa Sauvagei, Int. J. Peptide Protein Res. 17 (1981) 275–283.

[2] *M. Amiche, A. Delfour, P. Nicolas*, Opioid peptides from frog skin. EXS. 85(1998) 57–71.

[3] *G. Mignogna, C. Severinib, M. Simmacoa, L. Negric et al.* Identification and characterization of two dermorphins from skin extracts of the Amazonian frogvPhyllomedusa bicolor, Febs Letters, 302 (1992) 151–154.

[4] *H. Choi, T.F. Murray, J.V. Aldrich.* Dermorphin-based potential affinity labels for mu-opioid receptors, J Pept Res. 61 (2003) 40-45.

[5] *P. Melchiorri, L. Negri,* The dermorphin peptide family, Gen. Pharmacol. 27 (1996) 1099–1107.

[6] *M. Broccardo, V. Erspamer, G.Falconieri Erspamer et al.,* Pharmacological data on dermorphins, a new class of potent opioid peptides from amphibian skin, Br. J. Pharmacol. 93 (1981) 625–631.

[7] *W. Bogdanich* " Turning to Frogs for Illegal Aid in Horse Races", New York Times. Retrieved 19 June 2012.

[8] *G. Kreil.* Peptides containing a D-amino acid from fogs and molluscs, J. Biol. Chem. 269 (1994) 10967–10970.

[9] *S.D. Heck, W.S. Faraci, P.R. Kelbaugh, N.A. Saccomano, P.F. Thadeio, R.A. Volkmann*. Posttranslational amino acid epimerizations:

enzyme-catalyzed izomerization of amino acid residues in peptide chains, Proc. Natl. Acad. Sci. U.S.A. 93 (1996): 4036–4039.

[10] *M. Attilas, S. Salvadori, G. Balboni et.al.* Synthesis and receptor binding analysis of dermorphin hepta-, hexa- and pentapeptide analogues, Chemical Biology and Drug Design 42 (1993) 550-559.

[11] *S. Salvadori, G. Sarto, R.* Tomatis Syntesis and pharmacological activity of dermorphin and its N-terminal sequences, Int J Pept Protein Res. 19 (1982) 536-542.

[12] *K. Darlak, Z. Grzonka, P. Krzascik, S.W. Janicki* The role of side chains of amino acid residues on the biological activity of dermorphin, Peptides 5 (4) (1984) 687-689.

[13] *N.M. Godjayev, I.S. Maksumov, L.I. Ismailova.* Program of semiempirical calculations of conformations of molecular complexes, J.Struct.Chem., 4(1983) 147-148 (in Russian).

[14] *G.A. Akverdieva*. Improvement of program of calculation of molecular conformation. Theoretical and applied aspects of modern science. Collection of scientific papers of VI International Scientific-Practical conference, Belgorod (2015) 11-14. (in Russian)

[15] *J. Hermans and D. Ferro*. Representation of a protein molecule as a tree and application to modular computer programs which calculate and modify atomic coordinates, Biopolymers, 10(1971)1121-1129.

[16] *N.M. Godjayev, S. Akyuz, G.A. Akverdieva.* A molecular mechanics conformational study of peptide T, J. Mol. Structure 403 (1997) 95-110

[17] *G.A. Akverdieva, N.M. Godjayev, S. Akyuz*. Conformational dynamics of peptide T molecule. Journal of Molecular Structure, 609 (2002) 115-128.

[18] IUPAC-IUB. Quantities, Units and Symbols in Physical Chemistry, Blackwell Scientific, Oxford (1993) 168.

[19] *K.V. Shaitan, S.S. Saraykin*. Molecular dynamics method, 1999. http:// www.moldyn.ru (in Russian)

[20] *H.W. Horn, W.C. Swope, J.W. Pitera et al.* Development of an improved four-site water model for biomolecular simulations: TIP4P-Ew. J. Chem. Phys. 120 (2004) 9665-9678.

[21] *N.L. Allinger, Y. Yuh.* QCPE 395, Quantum chemistry program exchange, Indiana Univ., Indiana, 1982.

[22] *G.A. Akverdieva*. Molecular mechanics study of [D-Arg2] – dermorphin tetrapeptide analogues. 5-th International Conference on Biological Physics (ICBP) 2004, August 23-27, Gothenburg, Sweden, p.89, B05-158.

[23] *G.A. Akverdieva, N.S. Nabiyev, N.M. Godjayev, U.T. Eminzade.* Structure-functional relationship of the dermorphin tetrapeptide analogs, Baku University News, Ser. of Physical and Mathematical Sciences, 3(2005)197-203(in Azerbaijan).

[24] *N. Pattabiramann, K. Sorensen, R. Langridge et al.* Molecular mechanics studies of dermorphin, Biochem. Biophys. Res. Commun. 140 (1986) 342-349.

[25] *A. Pastore, P.A. Temussi, S. Salvadori.* A conformational study of the opioid peptide dermorphin by one- dimensional and two-dimensional nuclear magnetic resonance spectroscopy, Biophysical Journal 48 (1985) 195–200.

[26] *E. Arlandini, M. Ballabio, R. De Castiglione et al.* Spectroscopic investigations on dermorphin and its [L-Ala2] analog, Int.J.Pept. and Protein Res. 25 (1985) 33-46.

[27] *F. Toma, V. Dive, S. Fermandjian, K. Darlak et al.* Preferred solution and calculated conformations of dermorphin and analysis of structure-conformation-activity relationships in the series [Ala]-dermorphin, Biopolymers 24(1985) 2417-2430.

[28] *G. Ranghino, C. Tosi, L. Barino et al.* Conformational properties of the analgesic peptide dermorphin and their relationships to biological activity, J. Mol. Structure (THEOCHEM), 164 (1988) 153-164.

[29] *V. Renugopalakrishnan, R.S. Rapaka*. Conformational studies of dermorphin, NIDA Res. Monogr. 87(1988) 74-82.

[30] *M. Segawa, Y. Ohno, M. Doi.* Comparative conformational analyses of mu-selective dermorphin and delta-selective deltorphin-II in aqueous solution by 1H-NMR spectroscopy. Int J Pept Protein Res. 44(1994)295-304.

[31] *M.D.Shenderovich, I.T.Liyepinya, G.V. Nikiforovich*. Conformation-function relationships for dermorphin and its pentapeptide analogues, J.Bioorganic Chemistry, 15 (9) (1989) 1161-1172. (in Russian)

[32] *G.A. Akverdieva*. Structure-dynamical properties of dermorphin (in Azerbaijan). Journal of Qafqaz University, 32(2011)7-12.

[33] *L.H. Lazarus, W.E. Wilson, A. Guglietta, R. De Gastiglione*. Dermorphin interaction with rat brain opioid receptors: involvement of hydrophobic sites in the binding domain, Molecular Pharmacology 37(1990) 886-892.

[34] *N.E. Kuzmina, V.A. Yashkir, V.A. Merkulov and E.S. Osipova*. The estimation method of compounds opiate activity based on universal three-dimensional model of the nonselective opiate pharmacophore. J.Bioorganic Chemistry 38(5)(2012)577-590. (in Russian)

[35] *A. Tavani, L.E. Robson, H.W. Kosterlitz.* Differential postnatal development of μ-, δ- and k-opioid binding sites in mouse brain, Development Brain Research 3(1985) 306-309.

[36] *I.D. Pogozheva, A.L. Lomize, H.I. Mosberg.* Opioid receptor three-dimensional structures from distance geometry calculations with hydrogen bonding constraints, Biophys. J. 75 (1998) 612-634.

Received: 15.02.2016

COMPARATIVE STUDY ON THE ELECTRICAL CHARACTERISTICS OF Au/n-Si AND Au/P3HT/n-Si DIODES

A.ASIMOV[a], A. KIRSOY[b]

[a]Institute of Physics, Academy of Sciences of Azerbaijan, 33 H. Javid, Baku Azerbaijan– 1143
[b]Department of Physics, Faculty of Sciences and Arts, Uludag University,
16059 Gorukle, Bursa, Turkey
Corresponding author: E-mail address: fizikasimov@gmail.com Tel: 518991515

In this work, we have fabricated Au/P3HT/n-Si and Au/n-Si Schottky barrier diodes (SBDs) to investigate the effect of polymer interfacial layer on the electronic parameters. Electronic parameters of these two diodes were calculated from the currente-voltage characteristics. It was seen that the ideality factor value of 3.47 eV calculated for the Au/P3HT/n-Si device was higher than the value of 1.18 eV of the Au/n-Si Schottky diodes. The R_s values obtained from Cheung's function are 18.6 and 495 for Au/n-Si and Au/P3HT/n-Si, respectively.

Keywords: Metal semiconductor-structure , conductive polymer, P3HT, ideality factor
PACS: 6855 jk

1. INTRODUCTİON

Conductive polymeric materials have advantages such as, a good mechanical flexibility, high hole mobility, stable in the atmosphere and easy fabrication [3–5]. There has been much interest in the conductive polymeric materials in the study area of solar cells, light emitting diodes and thin film transistors. Among the conducting polymers, P3HT has specific properties such as a good mechanical flexibility, high hole mobility and is stable in the atmosphere. The electronic parameters of the diodes such as the ideality factor, the barrier height, the interface state density, the thickness of the interfacial layer and series resistance (R_s) from current–voltage (I–V) and capacitance–voltage (C–V) measurements [6-10]. In this study, we will fabricate the Au/P3HT/n-Si metal/polymer/semiconductor (MPS) device by spin coating method.

2. EXPERİMENTAL PROCEDURES

n-Type Si semiconductor wafer with (100) orientation and 280 mm thickness was used before making contacts, the wafer was chemically cleaned using the RCA cleaning procedure (i.e.10 min boil in $H_2SO_4 + H_2O_2$ followed by a 10 min $HCl + H_2O_2 + 6H_2O$ at 60 ^{0}C). The ohmic contact with a thickness of ~1500 Å was made by evaporating 99.9% purity Au metal on the back surface of the n-Si substrate, then was annealed at 550 °C for 3 min in N_2 atmosphere. Front surface of samples were coated with a conducting polymer poly(3-hexylthiophene) (P3HT) (fig.1) film by spin coating (VTC-100) with 1200 rpm for 60 s. After that rectifier Schottky contacts were formed on the other faces by evaporating ~2000Å thick Au. The I−V measurements were performed using a Keithley 6517A electrometer and C−V measurements were carried out at room temperature with a Keithley HP-4194 C−V Analyzer.

3. ANALYSİS OF Au/P3HT/n-Si JUNCTİON DİODE AT ROOM TEMPERATURE

The forward-and reverse-bias I–V characteristics of the Au/P3HT/n-Si contact and are ference Au/n-Si diode at room temperature are shown in fig. 1. As clearly seen from fig. 1, the Au/P3HT/n-Si structure exhibits a good rectifying behavior. We analyze the experimental I–V characteristics by the forward bias thermionic emission (TE) theory given as follows [1-2]

$$I = I_0 \exp\left(\frac{q(V-IR)}{nkT}\right)\left[1-\exp\left(\frac{-q(V-IR)}{kT}\right)\right] \quad (1)$$

where

$$I_0 = AA^*T^2 \exp\left(-\frac{q\phi_{b0}}{kT}\right) \quad (2)$$

is the saturation current, Φ_{b0} (I-V) is the zero bias barrier height, A* is the Richardson constantant and equals to 120 $Acm^{-2}K^{-2}$ for n-type Si, where q is the electron charge, n is the ideality factor. From eq.(1), ideality factor n can be written as

$$n = \frac{q}{kT}\left(\frac{dV}{d(\ln I)}\right) \quad (3)$$

n equals to one for an ideal diode. However, n has usually a value greater than unity. High values of n can be attributed to the presence of the interfacial thin native oxide layer and a wide distribution of low-SBH patches (or barrier height inhomogeneities), and, therefore, to the bias voltage dependence of the SBH [1-2]. Fig.1 presents the forward bias current–voltage (I–V) characteristics of the Au/P3HT/n-Si/Au structure. The Φ_{b0} and n values of these diodes were calculated from a linear fit of the *lnI* vs *V* plots in fig. 1 by using the eqs. (2) and (3) and the obtained values are 0.78 eV and 1.18 for Au/n-Si/Au diode, 0.75 eV and 3,47 for Au/P3HT/n-Si/Au diode, respectively. It has been observed that ideality factor of Au/P3HT/n-Si structure increases about 2.29 with respect to Au/n-Si at room temperature.

131 H.Javid ave, AZ-1143, Baku
ANAS, G.M.Abdullayev Institute of Physics
E-mail: jophphysics@gmail.com

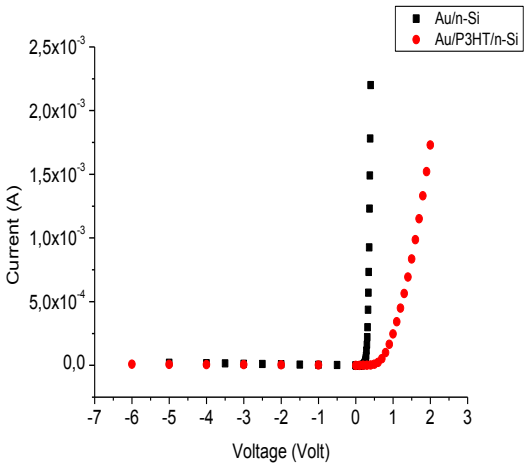

Fig 1. The forward and reverse bias semi-logarithmic I–V characteristics of Au/n-Si and Au/P3HT/n-Si Schottky barrier diodes at room temperature.

The value of the ideality factor is greater than unity. The high values in the ideality factor are caused possibly by various effects such as inhomogeneities of P3HT film thickness, non-uniformity of the interfacial charges and series resistance, [11-14].

The values of the series resistance is determined from following functions using eq. (4).

$$\frac{dV}{d(\ln I)} = IR_s + n\left(\frac{kT}{q}\right) \qquad (5)$$

$$H(I)=V-n\left(\frac{kT}{q}\right)\ln\left(\frac{I_0}{AA^*T^2}\right) \qquad (6)$$

In fig. 2 (a) and (b), the values of *dV/d(ln I)–I* and *H(I)–I* are plotted for Au/P3HT/n-Si and Au/n-Si Schottky contacts , respectively. A plot of *dV/dln(I)* vs *I* will gives R_s as the slope and n the y-axis intercept [15]. The values of n and Rs for SBD were derived from fig. 2 by using eqs. (5) and (6), respectively, and they were presented in Table 1. The R_s values obtained from eq. (5) are 18.6 and 495 for Au/n-Si and Au/P3HT/n-Si, respectively. The high series resistance R_s value can be attributed to the presence of a native interfacial layer between metal and semiconductor. The interface states and interfacial layer between the metal/semiconductor structures play an important role in the determination of the electronic parameters of the diodes. Density of interface states proposed by Card and Rhoderick can be simplified and given as [13;14]:

$$N_{ss}(V) = \frac{1}{q}\left\{\frac{\varepsilon_i}{\delta}[n(V)-1] - \frac{\varepsilon_s}{W_D}\right\} \qquad (7)$$

where N_{ss} is the density of the interface states, δ is the thickness of interfacial layer, W_d is the space charge width, and *n(V)* is the voltage-dependent ideality factor, $\varepsilon_s=11.8\varepsilon_0$ and $\varepsilon_i=3\varepsilon_0$ are the permittivity of the semiconductor and conducting polymer (P3HT), respectively. In n-type semiconductors, the energy of the interface states E_{ss} with respect to the bottom of the conduction band at the surface of the semiconductor is given by

$$E_c - E_{ss} = q(\Phi_e - V_D) \qquad (8)$$

Where V_D is the applied voltage drop across the depletion layer and Φ_e is the effective barrier height. N_{ss} values are obtained via eq.(11). Fig. 3 shows the energy distribution profiles of N_{ss} extracted from the forward bias I–V characteristics for Au/P3HT/n-Si and Au/n-Si Schottky barrier diodes . The magnitude of N_{ss} ranges from 5.05x10^{11} at Ec—0.63 eV to 2.01x10^{12} eV^{-1} cm^{-2} at Ec—0.46 eV for Au/P3HT/n-Si SBD and 5.46x10^{11} at Ec—0.61 eV to 6.33x10^{11} eV^{-1} cm^{-2} at Ec—0.47 eV for Au/n-Si Schottky barrier diodes.

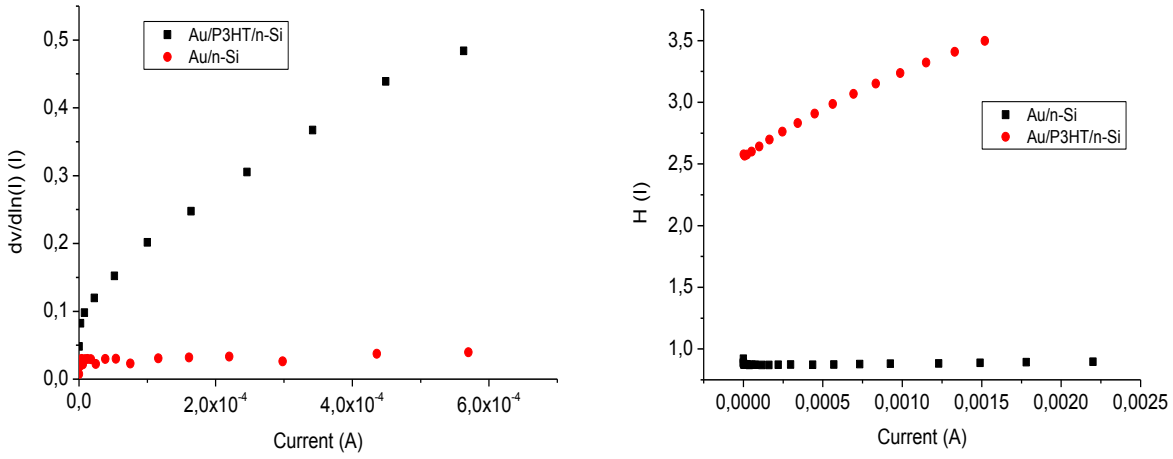

Fig 2. The plots of dV/d ln I and H(I) vs. current of Au/n-Si and Au/P3HT/n-Si Schottky barrier diodes at room temperature.

Table 1.

The experimental values of some parameters obtained from the forward bias I–V characteristics of Au/n-Si and Au/P3HT/n-Si Schottky barrier diodes at room temperature.

Diodes	n	Φ_b	I_o	dV/dLn(I)		H(I)		N_{ss}
				N	R_s	R_s	Φ_b	
Au/n-Si	1,18	0,78	7,56e-9	1,12	18,6	13,5	0,73	$6,3x10^{11}$
Au/P3HT/n-Si	3,47	0,75	2,08E-8	6,07	495	611	0,74	$2,1x10^{12}$

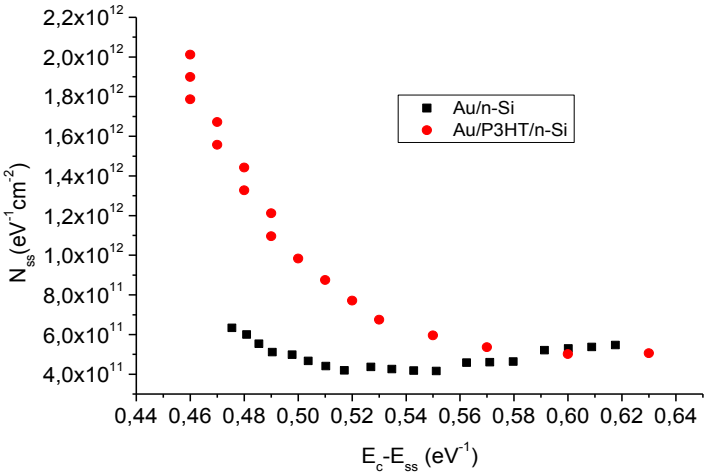

Fig. 3. The energy distribution profiles of N_{ss} for Au/n-Si and Au/P3HT/n-Si Schottky barrier diodes at room temperature.

IV. CONCLUSION

Electronic properties of the Au/n-Si and Au/P3HT/n-Si Schottky barrier diode have been investigated by means of I–V measurements at room temperature. It was seen that the ideality factor value of 3.47 eV calculated for the Au/P3HT/n-Si device was higher than the value of 1.18 eV of the Au/n-Si Schottky barrier diodes. The values of the ideality factor, series resistance and barrier height obtained from Cheung and Norde method were compared, and it was seen that there was an agreement with each other.

[1] *S.M. Sze*. Physics of Semiconductor Devices, 2nd ed., John Wiley & Sons, New York, 1981.

[2] *E.H. Rhoderick, R.H. Williams.* Metal–Semiconductor Contacts, Clerendon, Oxford, 1988.

[3] *T. Tunç, İ. Uslu, İ. Dökme, Ş. Altındal, H. Uslu*. International Journal of Polymeric Materials (2010)

[4] *F. Yakuphanoglu*. Synthetic Metals 160 (2010) 1551–1555.

[5] *P. Anuragudom, J. El-daye, P. Chinwangso, R.C. Advincula, S. Phanichphant, T.R. Lee*. Polymer International 60 (2011) 660–665.

[6] *Ahmed Fatime E, Yassin OA.* Microelectron J 2007; 38:834.

[7] *F. Yakuphanoglu.* J. Alloys Compd. 494 (2010) 451e455.

[8] *Nguyen N.C, Potje-Kamloth K.* Thin Solid Films 1999;338:142.

[9] *W. Brütting.* Physics of Organic Semiconductors, Wiley-VCH-Verlag GmbH & Co.KGaA, Weinheim, 2005.

[10] *E.J. Meijer, A.V.G. Mangnus, C.M. Hart, D.M. de Leeuw, T.M. Klapwijk.* Appl. Phys. Lett. 78, (2001).

[11] *F. Yakuphanoğlu, M. Shah and W. Aslam Farooq.* A. Phys. Polonica A 120 (2011) 3

[12] *E. Voroshazi, B.Verreet, T.Aernouts, P.Heremans*. Solar Energy Mater. Solar Cells 95 (2011) 1303–1307.

[13] *Norde H.* J. Appl. Phys. 1979;50:5052.

[14] *H.C. Card, E.H. Rhoderick.* J. Phys. D: Appl. Phys. 4 (1971) 1589.

Recevied: 26.04.2016

INVESTIGATION OF ANALYTIC CHARACTERISTICS OF MASS-SPECTROMETER WITH INDUCTIVELY COUPLED PLASMA "AGILENT-TECHNOLOGIES 7700 İCP-MS"

T.K. NURUBEYLI
Institute of Physics of Azerbaijan Az-1143, H.Javid ave.,131, Baku
omartarana@gmail.com

The main characteristics of mass-spectrometer with inductively coupled plasma of "Agilent-Technologies 7700 İCP-MS" (USA) firm are investigated. It is shown that device has enough wide range of calibration linearity (up to 5 orders of concentration changes of investigated elements). The ion composition of inductively coupled plasma mainly consists of singly ionized ions as distinct from laser and spark mass-spectrometers that gives the possibility of etalon-free analysis of solid substances. The measured sensitivity of mass-analyzer isn't worse than 100 ppb. The measuring accuracy of several metals doesn't exceed S=0,003 at right choice of devise mode.

Keywords: plasma, laser and spark mass-spectrometers, etalon-free analysis, inductively coupled plasma, single and double charge, quadrupole and etc.
PACS: 07.75.+h

INTRODUCTION

The mass-spectrometry with inductively coupled plasma (ICP-MS) is widely adopted for analysis of both inorganic and organic substances. The water solutions are analysis objects in ICP-MS in many cases. The solid samples are solved in nitric or hydrochloric acids (2-5%) and later they are analyzed.

Such popularity PCP-MS method has gained by the fact that here these processes are divided from each other by time and space as distinct from ionization process by laser and spark methods where laser impulse energy (or vacuum spark discharge) is given to dissociation and ionization of sample elements that leads to energy variation of analyzed ions. That's why the energies of different ions differ. Indeed, the ions of different elements having the different dissociation energies (W_a) and potentials of single and double ionizations lose the different energies $\varphi_a+\varphi_i$ in spite of the fact that they gain the similar energy during laser impulse.

The quite opposite situation is in ICP-MS. The sample long before measurements is dissolved in 2% nitric acid (or hydrochloric one in dependence on sample chemical composition) where the substance divides into atoms of substance elements, further the solution is put into sprayer and there it transforms into aerosol with the help of argon. The aerosol being in argon plasma ionizes under influence of high temperature of inductive plasma. Thus, processes of dissociation and ionization of elements almost separated from each other in ICP-MS and ions leaving the plasma have the energy variation ($\Delta W<10eV$) not exceeding the ionization energy of different element atoms.

The more detail investigation of main parameters of both mass-spectrometer with inductively coupled plasma and their comparison with analogous parameters of laser and spark spectroscopy is the aim of present paper.

EXPERIMENTAL PART

Experiment condition: *Ion source*: ICP-MS type; inductor, consisting of three turns to which the voltage of high frequency 27,12*MHz* by power 1,2*kW* in standard mode is applied; the average temperature of plasma is 8000-7000K. The so-called interface is used at constant evacuation for transition of ion flux from plasma being under the pressure near 0,1*bar* in vacuum part of mass-spectrometer in which the pressure is 10^{-5}-10^{-7} *mbar*.

Investigated samples. The samples are chosen so that one can cover the major number of parameters on the base of limited quantity of experiments, in particular, such as consistency (compact samples, thin layers); melting point (easy-evaporating and refractory materials).

It is known that the definition of chemical composition of solid substances by mass-spectrometry method is based on division of ions of investigated substance in electric or magnetic fields. For ionization of these substances the energy is applied by different ways (laser and spark ions with high energy and etc). This energy consumes on dissociation and ionization of atoms of investigated substance.

The general scheme of mass-spectrometer with inductively coupled plasma is shown in fig.1. It consists of the system of sample introduction consisting of peristaltic pump **1** and sputtering chamber **2** supplied by pneumatic sprayer **3**; plasma burner block **4**, which is connected to extraction ventilation for ozone elimination forming from the atmospheric oxygen under ultraviolet influence, products of sample decomposition and released heat; interface part **5,** extractor **6**, serving for ion taking from plasma and their transportation into high-vacuum part of mass-spectrometer ; deflection system **7**, ion optics system **8**, quadrupole mass-analyzer **9**, ion detector (SEM) **10**.

Moreover, ionization mode is chosen so that ion charge doesn't exceed the one-and two-multiplicity. The formed positive charged ions goes through ion optics system into mass-analyzer where the ion division by mass and detection takes place.

The quadrupole (fig.2) presents itself the parallel and symmetrically posited four rods to which the combination of constant and high-frequency voltage is applied in pairs. Moreover, the ion division by mass takes place in dependence on alternating voltage frequency.

131 H.Javid ave, AZ-1143, Baku
ANAS, G.M.Abdullayev Institute of Physics
E-mail: jophphysics@gmail.com

$$M_i = \frac{a(U_0)}{\omega^2}$$

where U_0 is constant voltage amplitude, ω is high-frequency voltage, a is instrument constant.

The experimental investigations show that the output in one-, two- and more multiply charged ions depends on laser radiation parameters (wave length, pulse duration, power and etc) in laser mass-spectrometers.

The majority of ions in inductively coupled plasma is singly charged as distinct from laser and spark plasmas. The high temperature of argon plasma in such devices allows ionizing the atoms of all elements of periodic system with first ionization potential up to 15,76 *eV* (the potential of single ionization of *Ar* atoms). However, the formation of double charged ions and elements having the low second ionization potentials is possible in ICP-MS. The experiments show that series of (*Be*, *Ca*, *Sr*, *Ac*, *Sc*, *Ga*) elements have the least secondary potentials and the appearance of M^{++} is very often observed especially for these elements. Bur such ions as *Pb* ($\varphi_i^{++} = 15{,}03\ eV$), *Mg* ($\varphi_i^{++} = 15{,}13\ eV$) and *Mn* ($\varphi_i^{++} = 15{,}64\ eV$) have the small intensity in mass-spectra.

Consequently, the almost third part of periodic table elements is the potentially dangerous by formation of double charged ions. The presence of M^{++} in ICP-MS leads to intensity decrease of M^+ ion signals though it is considered that if $M^{++}/M^+<5\%$ so the decrease of intensity peak of M^+ is insignificant one [1,2]. That's why the definition of ratio M^{++}/M^+ of separate elements plays the essential role in calculations of concentration of these elements by measured mass-spectrum.

If we suppose that the thermo-dynamic equilibrium takes place in ICP-MS plasma, then the formation efficiency of double-charged ions (M^{++}) which depends on ion ionization second potential (φ_i^{++}) one can obtain by Sakha equation [3]:

$$\frac{M^+}{M^0} = \left(\frac{2\pi mT}{h^3}\right)^{3/2} \cdot \frac{2Z_i^+(T)}{Z_i^0(T)} \cdot \frac{1}{n} exp\left(-\frac{e\varphi_i^+}{kT}\right) \quad (1)$$

$$\frac{M^{++}}{M^+} = \left(\frac{2\pi mT}{h^3}\right)^{3/2} \cdot \frac{2Z_i^{++}(T)}{Z^+(T)} \cdot \frac{1}{n} exp\left(-\frac{e\varphi_i^{++}}{kT}\right) \quad (2)$$

where m, n are mass and concentration of electron; h is Planck constant; k is Boltzman constant; $Z_i^0(T)$, $Z_i^+(T)$ and $Z_i^{++}(T)$ are sums over states of atom, single and double charged ions at T temperature correspondingly.

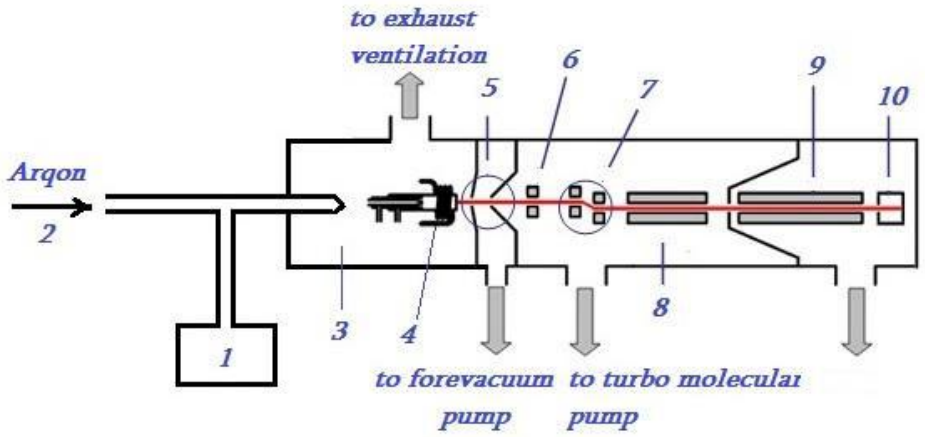

Fig.1. The general scheme of mass-spectrometer with inductively coupled plasma.

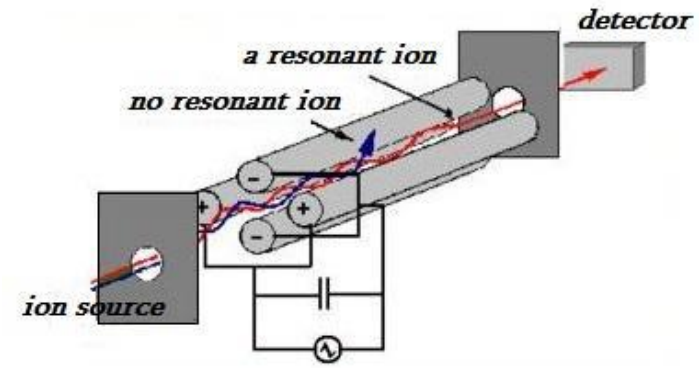

Fig.2. The scheme of quadrupole mass-analyzer.

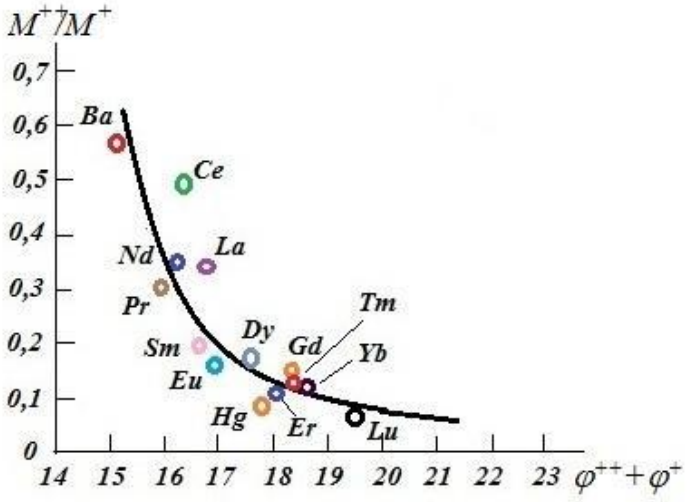

Fig 3. The experimental relation of M^{++}/M^{+} ion concentrations in dependence on sum of first and second potentials of atom ionization.

THE RESULTS AND DISCUSSION

As it is above mentioned the presence of M^{++} ions in ICP-MS of defined elements decreases the analytical signal of M^{+} of given elements (M^{+}) and, therefore, makes worse their detection limit. Simultaneously, the presence of M^{++} ions of corresponding elements (especially, if their concentrations are high ones) leads to disturbance appearance [4].

That's why in modern devices ICP-MS the index M^{++}/M^{+} is the main to characterize of technical feasibilities of devices and it is established by Ce^{++}/Ce^{+}=1% or Ba^{++}/Ba^{+}=3%, especially by this relation of analytical signals on output of the given elements(Ce^{++}, Ba^{++}) the device tuning of working mode is carried out.

At development of concrete analysis method with ICP-MS help, it is necessary to take into consideration the possibility of M^{++} mass-spectrum appearance and moreover, one can orientate on regularities of their formation in inductive plasma. About 20 pure elements having the different energies of dissociation and first ionization potential are investigated by us. The coincidences of experimentally obtained relations of concentrations of double-charged ions to one-charged ones on sum of first and second ionization potentials ($\varphi_i^{+} + \varphi_i^{++}$) are given in fig.3. φ_i^{+} and φ_i^{++} are taken from [5].

From the figure it seen that the type of functional dependence $M^{++}/M^{+}=f(\varphi_i^{+} + \varphi_i^{++})$ is observed enough definitely. The study of reference [5-7] on M^{++} ion formation where the significant scatter of readings shows that the observable high relations of M^{++}/M^{+} are connected with the appearance of second discharge (breakdown) between plasma having the definite high potential and grounded construction elements. The many experiments show that plasma potential depend on such parameters as argon flow rate [6], discharge power and inductor connection method.

M^{++}/M^{+} relation is defined by ion energy, increases with plasma potential increasing, argon central flow rate increasing and discharge power decreasing.

The measurements are carried out in ICP-MS of firm "Agilent-Technologies 7700" (USA). Note that the calibration wide range is the distinctive characteristics of the given type of mass-spectrometer. That's why the device calivration is carried out up to 5 orders of concentration change ($n \cdot 10^{5}$ cm^{-3}) in dependence on chosen condition. *Cu, Ag, Ni, Al, Zn, Mo, W* and etc are used as samples. These samples are solved in 2% nitric acid, further they are injected in plasma. The internal standards are used at element analysis of solid substances. In ideal case the internal standard on physicochemical properties (atomic mass, ionization potential and etc) should be close to analyte. The following elements: ^{6}Li, ^{45}Sc, ^{72}Ge, ^{103}Rh, ^{115}In, ^{175}Lu are used as internal standards.

The soil taken from the parts adjacent to oil fields is examined for the revealing the heavy metals in their compositions.

The device calibration with the help of following elements with participation of above mentioned internal standards: *Mg, Al, Cr, Mn, Fe, Co, Cu, Ni, As, Zn, Mo, Pb* is carried by us at preparation of analysis sample of soil composition polluted by petroleum products. The calibration is carried out from *1 ppb, 5 ppb, 10 ppb, 20 ppb* and*40 ppb*. The 4 calibration curves for *Cu, Cr, Co* and *Ni* are given for example in fig.4. The straight lines in fig.4 show on the calibration regularity.

The samples taken from the different soil depths polluted by petroleum products before the analysis on mass-spectrometer are treated by the following way. The soil taken from each depth, is divided into 4 parts. The first part is solved in 60% nitric acid (sample 1), the second part is treated by constant voltage U=8kV and 14kV after pure water washing and ozonized water purification.

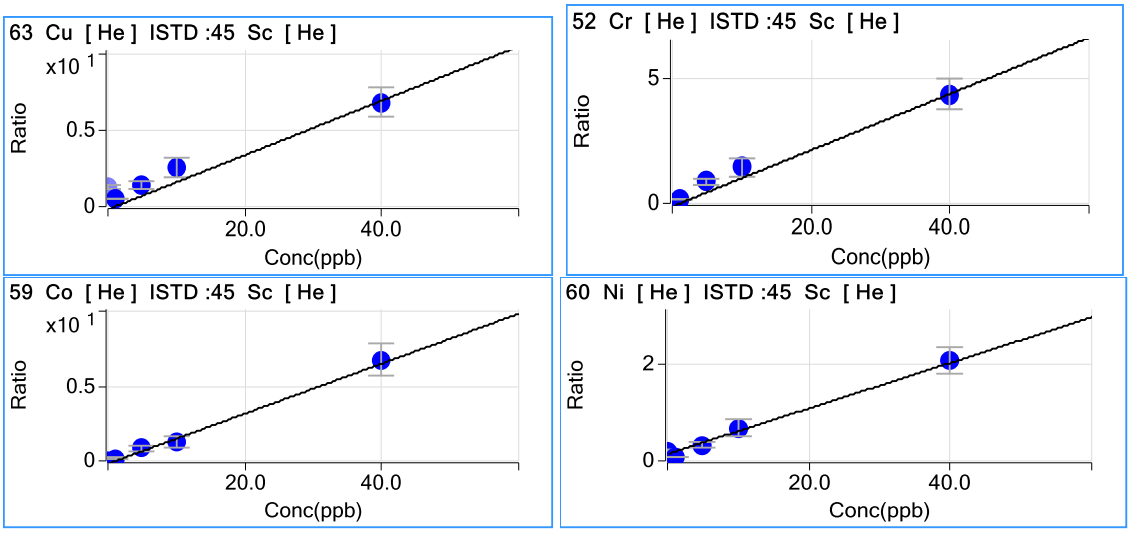

Fig.4. The element calibration in internal standard.

Table 1.

The concentrations of several elements consisting in soil after treatment.

Metal	The analysis of initial sample, ppb	The purifica-tion by water, ppb	The purification by ozonized water, U = 8kV		The purification by ozonized water, U =14κV		The purification by water, U = 14κV
			ppb, t=15min	ppb, t=30min	ppb, t=15min	ppb, t=30min	ppb, t=30min
Pb(0-10cm)	4,927	1,290	0,703	1,099	3,140	4,576	
Pb(10-20cm)	4,536	5,738	-	6,534	3,068	1,434	1,594
Ni(0-1cm)	7,112	2,520	2,580	1,985	1,231	1,630	
Ni(10-20cm)	6,070	3,710	-	3,196	1,349	1,200	1,344
Cu(0-10cm)		3,427	3,830	2,395	3,697	3,113	
Cu(10-20cm)		8,407	-	13,364	3,405	4,085	3,867
Mo(0-10cm)	164,178	35,766	42,224	6,584	19,564	20,521	
Mo(10-20cm)	331,694	30,364	-	25,395	22,536	22,662	20,521
Al(0-10cm)	528,248	72,757	149,119	215,68	222,047	258,435	
Al(10-20cm)	583,065	276,400	-	185,920	246,153	148,102	118,889

Further, the soils treated by electric field (samples №2 and samples №3) are separately solved in 60% nitric acid and their mass-spectrometric analysis is carried out.

The analysis results, i.e. the ion concentrations of several metals being in the soil composition, are given in table. The depths, from which the soils are taken for the analysis, are given in brackets after metal names.

The element concentrations are measured in ppb, i.e. the device sensitivity is from 10-100 *ppb* with accurate within 10^{-3} *ppb*. This shows the high sensitivity and resolution of device.

Result regularity. It is known that the one- (M^+) and double-charged (M^{++}) ions dominate in laser and spark mass-spectrometers [7,8]. That's why this fact presents the interest of definition of relative sensitivity factor (RSF) on lines of both one- (RSF_i^+) and double-charged ions by mass spectrum obtained in ICP-MS. The experiments on definition of M^{++}/M^+ relation are carried out for the several pure metals. Moreover, the plasma composition corresponds to experiment requirements and is $Ar^+ + M^+ + H_2O$. The argon consumption through pneumatic sprayer doesn't exceed 1l/min. The sample solution feed rate is 1l/min, the spray-type system efficiency is 0,02, the analyte composition is 10mg/l. *Cu, Ni, Zn, Al, Cr, Mn, Fe, Mg* are used as analyte.

RSF calculated by experimentally measured lines of above mentioned pure metals by following formula [7]:

$$RSF^x_{in.st.} = \frac{J_x}{J_{in.st}} \cdot \frac{n_{in.st.}}{n_x}$$

are given in table 2.

From the table it is seen that the calculation by cuprum lines gives RSF value close to 1 for both one-and double-charged ions.

Table 2.

The relative sensitivity factor calculated by results of measured concentrations of pure metals.

Elements	$n_x^+ \cdot 10^8 cm^{-3}$	$n_x^{++} \cdot 10^6 cm^{-3}$	RSF_i^+	RSF_i^{++}
Al	159	42	1,68	3,57
Cu	345	125	1,41	2,61
Ni	2415	512	1,16	4,73
Zn	450	315	1,43	0,95
Cr	178	2140	2,12	1,21
Mn	367	164	1,71	2,7
Fe	213	95	2,07	0,63
Mg	47	161	6,95	0,38

For one-charged ions the relation of maximum RSF_i^+ to minimum one is 2,5, i.e. the value range is approximately better on order than in laser and spark mass-spectrometry ($RSF_{max}^+/RSF_{min}^+=17,5$). The value range of this relation for two-charged ions is equal to 12,5. Therefore, the lines of these ions are less suitable for etalon-free analysis than lines of one-charged ions. Note that sometimes one should use the double-charged ions at analysis with application of internal standards.

Thus, the regularity of etalon-free analysis carried out on CP-MS, changes from matrix to another one and in general, it is comparable with regularity of laser and spark mass-spectrometry. Probably, changing the influence conditions on sample (frequency and power of high-frequency voltage) one can chose the conditions for which $RSF_{in.st.}^x$ values are more close ones for the definite matrix class.

CONCLUSION

1. The enormously wide range of linear calibration is the distinctive characteristics of mass-spectrometry with inductively coupled plasma. The calibration linearity is saved up to 5 orders of concentration change.
2. The regularity is about 2,5 (i.e. the relation $RSF_{max}^+/RSF_{min}^+=2,5$) at analysis on mass-spectrometer with inductively coupled plasma by lines of one-charged ions as at analysis by method of spark and laser mass-spectroscopy.
3. The device sensitivity ICP-MS for soil analysis is not less than 100 ppb.
4. The division of process of atomization and ionization by both the space and time in ICP-MS device allows us to use it for carrying out of etalon-free analysis of solid substances [9].

[1] *R.S. Houk.* Mass spectrometry of inductivity coupled plasma. Analytical chemistry 2004, v.56, №1/2, p.151-167.

[2] *A.A. Pupyshev, V.N. Muzgin, A.K. Lutsak.* Termochemical processes and ion transport in ICP-MS, theoretical disccription and exsperimental confirmation/ I of Analitical Atomic Spectrometry 1999, V.14, №9, p.1485-1492.

[3] *M.A. Elyashevich.* Atomnaya I molekulyarnaya spektroskopiya. M. Fizmatqiz, 1962, 892 s. (In Russian).

[4] *M.A. Vaughan, G. Hortick.* Oxide, hydroxide and double charged analyte species in ICP-MS// Applied Spectroscopy 2006 V.61, №4, p.434-445.

[5] *M.S. Chupaxin, O.I. Kryuchkova, Q.I. Ramendik.* Analiticheskie vozmojnosti iskrovoy mass – spektrometrii M. Atomizdat 1972, 224 s. (In Russian).

[6] *A.L. Gray, R.S. Houk, J.G. Williams.* J. of Analytical Atomic Spectrometry/ 1996. V.50 № 7, p. 971-973.

[7] *K.Z. Nuriev, Z.K. Nurubeyli, S.A.Manuchar, T.K. Nurubeyli.* Elektronnaya obrabotka materialov, 2011,t.47,№3, str. 85-89. (In Russian).

[8] *A.M. Qashimov, K.Z. Nuriev, K.B. Qurbanov, Z.K. Nurubeyli, S.A.Manuchar, T.K. Nurubeyli.* Jurnal texnicheskoy fiziki 2009, t. 79, № 8, s. 99-103. (In Russian).

[9] *Z.K. Nurubeyli, K.Z. Nuriev, T.K. Nurubeyli, K.B. Qurbanov.* Elektronnaya obrabotka materialov, 2015, t.51, №6, str. 78-84. (In Russian).

Recevied: 07.04.2016

MECHANICAL FAILURE KINETICS OF POLYMER COMPOSITIONS AT MODERATE AND LOW TEMPERATURES

I.K. ALIYEVA[1], P.B ASILBEYLI[2], M.J. TAGIYEVA[3]
[1]*Azerbaijan State Marine Academy, AZ 1005, Azerbaijan Republic, Baku, M.A. Rasulzade str.,5*
[2]*Institute of Physics of National Academy of Sciences of Azerbaijan, AZ1143,Baku, H.Javid ave.,131*
[3]*Ganja State University, Az 2000, H.Aliyev ave.,159*
e-mail: asilbeyli@mail.ru

The measurements of mechanical durability (rupture waiting time τ) for polymer compositions polypropylene-polyethylene of low density (PP-PELD) in temperature interval 90÷250K and at tension stress σ in interval 80÷110 MPa are carried out. The two region of $\tau(T)$ dependence are revealed at each constant σ value: well known $\tau(1/T)$ exponential dependence takes place at (~170÷250K) moderate temperatures; at low temperatures (~90÷170K) τ doesn't depend on T (temperature plateau). The conclusion to the fact that failure kinetics of polymer compositions is controlled by tunnel processes is made and the suppositions on possible tunneling mechanisms are given.

Keywords: polymer compositions, submolecular structure, electric failure, failure kinetics.
PACS: 81.05.Rm

INTRODUCTION

The conception of failure elementary acts of solids including the polymer compositions is introduced into physics of failure as a result of establishment of mechanical failure kinetic nature. The multiple systematic investigations show that failure is the kinetic phenomenon when in polymer substance the enough long process completing by the macroscopic rupture [1] develops from moment of load application.

The investigation of failure kinetics of solids at low temperatures, when the heat motion is weak and thermal fluctuations generated by it are rare ones, is in the beginning stage. The ideas on possibility of subbarrier (tunneling) mechanism of rupture of stressed interatomic bonds were given earlier [2,3]. The experimental investigations in which the dependence of failure stress on loading rate and temperature give the results coinciding with conception on tunnel rupture mechanism at corresponding low temperatures (below Debye ones) [4,5]. However, the direct measurement of temperature-force dependences of mechanical durability of polymer compositions isn't carried out.

The present paper is dedicated especially to this problem, as the registration of durability final values is the more convincing evidence of failure kinetic character and we can judge about the mechanism of failure elementary acts from temperature dependence of durability

THE OBJECTS AND MEASUREMENT TECHNIQUE

The investigation objects are optimal polymer compositions PP-PELD taken in ratio of components (PP-PELD=80:20) having different permolecular structures (PMS). The samples are taken in the form of films of thickness 20÷30μm. The length of working section is 10mm and width is 7mm.

The measurements of mechanical durability are carried out on tensile machine in which this or that values of temperature and tension stress are given for each sample and the time interval from load moment up to one of sample rupture is found. The sample deformation (tension) behavior during the time is also measured. The temperature is varied from ~ 90 up to 250 K. The durability is measured in time interval of several seconds up to 10^5 ones.

RESULTS AND THEIR DISCUSSION

The temperature dependence of durability at voltage constant for slow-cooling (SC) and rapid-cooling (RC) samples of PP:PELD polymer composition are shown in fig.1.

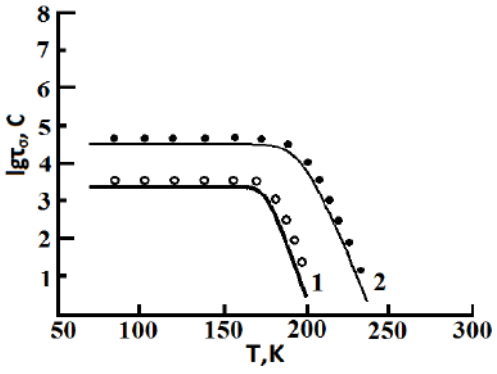

Fig. 1. Temperature dependences of mechanical durability of polymer compositions PP:PELD:
1 - SC samples, σ is 75 MPa;
2 - RC samples, σ is 85 MPa.

As it is seen from fig.1 $lg\tau(T)$ dependences for investigated polymer compositions are ones of the same type. The practical independence $lg\tau$ on T is observed in low temperature interval and this "plateau" is enough long-duration one (from 90 up to ~ 150-200 K). The

131 H.Javid ave, AZ-1143, Baku
ANAS, G.M.Abdullayev Institute of Physics
E-mail: jophphysics@gmail.com

strong decrease of durability takes place at moderate temperatures. Thus, two different regions of durability temperature dependence: athermal dependence and termosensitive one are revealed.

Let's present the obtained dependences in "hydrogen" coordinates $lg\tau - 1/T$ (fig.2) for their analysis.

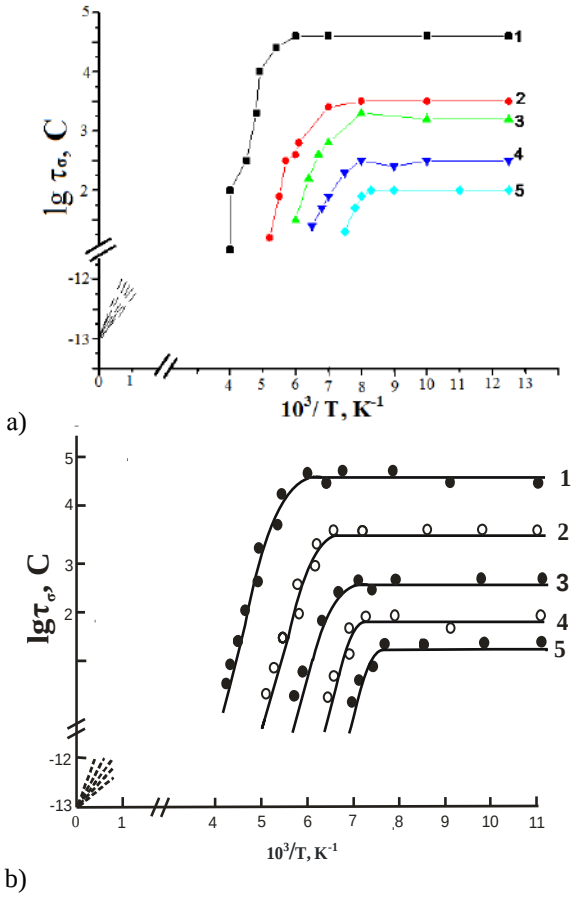

Fig.2. Temperature dependences of mechanical durability in hydrogen coordinates at different tension stress values for SC (a) and RC (b) samples of polymer compositions PP-PELD: a) 1is 80MPa , 4 is 95 MPa , 5 is 100 MPa; b) 1 is 85 MPa, 2 is 90 MPa , 3 is 95 MPa , 4 is 100 MPa , 5 is 105 MPa.

The dependences for each sample of polymer compositions at several tension stress values σ are shown (fig.2). The same two regions are revealed here: athermal and thermosensitive ones. The stress increase regularly decreases the durability in both regions. Besides, the stress influences on transition temperature from the one dependence to another: this temperature insignificantly decreases with stress increasing ("angle" on curves, fig.2). As it is seen from fig.2 $lg\tau$ $(1/T)$ dependence has the character close to linear one in thermosensitive region for durability investigated earlier in [1]. The extrapolation of $lg\tau$ $(1/T)$ to $1/T=0$ enough insignificantly leads to $lg\tau_0 \approx -13$ value. It gives the expression for durability in $\tau \approx \tau_0 \cdot exp[U(\sigma)/kT]$ form.

The physical meaning is that the failure kinetics of polymer and their compositions in given temperature interval is controlled by the static waiting of rupture act of stressed skeletal bonds in chain molecules by means of subbarrier (activation, thermo-fluctuation) bond transitions from associated state into dissociated one. In low temperature interval, where the durability dependence on temperature is absent (temperature "plateau"), the durability final values, regularly decreasing with stress increasing, are the evidence of that the failure process has the kinetic character, which is accelerated by means of the stress. The absence of the temperature dependence of durability indicates that the failure thermo-fluctuation (activation) mechanism of elementary acts doesn't take place.

The cases of experimental observation of low-temperature plateau for velocities of these reactions are noted in wide consideration of kinetics of solid-phase chemical reactions and it is shown that such plateau is connected with quantum nature, in particular, with tunneling of reaction elementary acts [6]. The rupture of stressed interatomic bonds is the one type of the chemical reactions in solid (reaction of destruction or dissociation).

The obtained data on "temperature plateau" for durability of investigated polymer compositions can have important mean as they show the possible change of failure mechanism of elementary acts at transition from moderate temperatures to low ones.

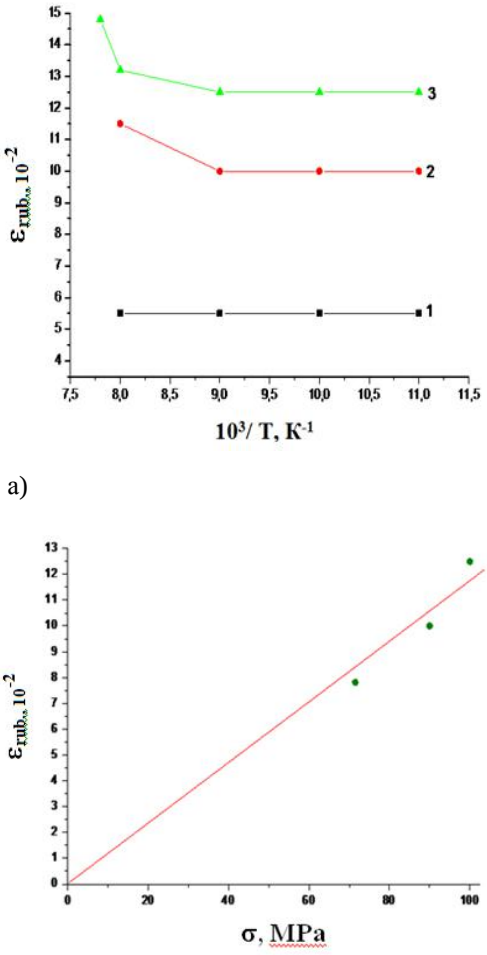

Fig.3. The rupture tension of SC samples of PP-PELD:
a) temperature dependences at σ= 75 MPa (1), 90 (2) and 100 MPa (3);
b) force dependence for low temperature interval.

The structure change of loaded samples due to plastic deformation of metals or polymer orientation exhaust leads to change of durability because of local condition changes of load action [1]. The deformability increase with temperature increasing for the polymer compositions can influence on the samples of polymer compositions and because of that the oriented structure appearance. It leads to composition hardening and durability increasing. Consequently, the singular compensation of thermo-fluctuation decrease of durability and increase of durability because of orientation takes place. The "plateau" similarity would take place but not only because of the change of failure mechanism.

The measurement of sample deformation (tension) from the application moment up to the rupture one is carried out for the purpose of the revealing of this question. In turns out that the sample rapid tension (fraction of a second) at application of constant load takes place in low temperature interval and further, the sample deformation in time remains practically constant up to its rupture. The level of this tension is proportional to load but it doesn't change with temperature in low temperature interval (fig.3).

The increase of sample elongation before the rupture with temperature is observed only at elevated temperatures. Thus, the observation of deformation low-temperature "plateau" (especially in this interval where "plateau" on durability is observed) allows us to consider that change of sample orientation state doesn't take place in low temperature interval.

Consequently the conclusion on the fact, that the athermal failure kinetics of investigated samples from polymer compositions takes place at low temperatures, has the additional experimental substantiations.

Thus, there is a conception to suppose that failure kinetics of given polymer compositions is controlled by tunneling processes in low temperature interval. The two types of tunneling processes leading to failure of polymer compositions can be given:

1) The tunneling ruptures of stressed polymer compositional molecules (atom chains) where the skeleton atom itself tunnels from the bound state through the dissociation barrier strongly increased by tension stress. Especially such process and its probability is considered in [7,8]. Note that such process is possible on principle and is enough obvious one at big tensile loads, i.e. the average waiting time can be accessible in laboratory conditions. The molecule ruptures at such transition mechanism from thermo-fluctuation (over-barrier) transition to tunneling (subbarrier) one take place at temperatures consisting in the definite part from the Debye temperature and depending on tension stress [8]. The tunneling of massive particles (atoms) occurs and tunneling kinetics of intrinsic failure of polymer compositions (accumulation of molecule tunneling ruptures) takes place in this processes. The data in fig.2 (a) and (b) corresponds to given change of molecule rupture mechanism as transition temperature on thermosensitive one to athermal kinetics regularly decreases with stress increasing as it follows from [8]. At the same time it is seen from fig.2 (a) and (b) that temperature intervals of these transitions for different samples of polymer compositions differ insignificantly, i.e. influence of PMC on these transitions is practically weak that gives the foundation for consideration of other tunneling process.

2) The preparation of stressed molecules to the rupture due to tunneling electron ionization.

There are experimental data showing the participation of electron processes in mechanical failure of polymers and their compositions. Thus, the acceleration of polymer mechanical failure and their compositions investigated in present paper at application of electrostatic field [9] is observed. The electron emission at polymer tension [10] is also revealed.

That's why one can give the following explanation of failure mechanism of polymer compositions in athermal region. As it is known if the polymer molecule ionizes so the rupture density of molecule section near the place of electron departure strongly decreases [11]. If we suppose that the electron tunneling output from skeleton atom in trap neighboring with molecule (inter-chain cavities) for strongly stressed macro-molecule becomes possible, then such ionized molecule will be rapidly failed. At such mechanism the rupture waiting time is controlled by the waiting of tunneling ionization act. The consideration of tunneling electron output from stressed polymer molecules at fluctuation local molecule tensions is given in [12].

CONCLUSION

The experimental observation of low-temperature plateau for mechanical durability of polymer compositions PP-PELD and also the supposition about possibility of tunneling process participation in failure kinetics and statement of question on concrete forms of these tunneling processes are the main conclusions of present paper.

[1] *A.I. Sluchker, V.I. Vetterqen, V.L. Qilyarov, Yu.I. Polikarpov*. FTT, 2007, t.49, №9, s.1608-1617. (In Russian).

[2] *J.J. Gilman, H.C. Tong*. Quantum tunneling as an elementary fracture process. J. Appl.Phys. 1971, v.42, p.3479-3486.

[3] *P.L. Salqanik.* Kinetika razrusheniya chepochecnix struktur. DAN SSSR, 1979, t.185, s.76-79. (In Russian).

[4] *A.I. Sluchker, V.L. Qilyarov, Yu.I. Polikarpov, D.D Karov*. FTT, 2010, t.52, №8, s. 1524-1530. (In Russian).

[5] *A.I. Slutsker, T.M. Veliev, I.K. Alieva, S.A. Abasov*. Kinetics of polymer failure at moderate and low temperatures. Makromol. Chem. Macromol. Sump. 1991, v.41, p.109-118.

[6] *V.I. Qoldanskiy, L.I. Traxtenberq, V.N. Flerov*. Tunnelnie yavleniya v ximicheskoy fizike. M: Nauka, 1986, 294s. (In Russian).

[7] *P.L. Salqanik.* FTT, 1970, t.12, №5, s.1336-1343. (In Russian).
[8] *M.I. Dyakonov.* FTT, 1987, t.29, №9, s.2587-2594. (In Russian).
[9] S.A. Abasov, M.A. Kurbanov, T.M. Veliev, M.M. Kuliev. FTT, 1982, t.24, №3, s. 693-695. (In Russian).
[10] *V.A. Zakrevskiy, V.A. Paxotin.* FTT, 2010, t.52, №6, s.1083-1089. (In Russian).
[11] Energiya razriva ximicheskix svyazey, potenchiali ionizachii i sredstvo k elektronu. *Pod. red. V.N. Kondrateva.* M:Nauka, 1974, 352 s. (In Russian).
[12] *A.I. Qubanov.* Rachet lokalnoqo elektronnoqo urovnya v razrivaemoy molecule polietilena. Mexanika polimerov, 1978, №5, s.771-775. (In Russian).

Received: 16.02.2016

THE INFLUENCE OF PRIMARY STRUCTURE OF *LEU*-CALLATOSTATINES 1 AND 2 ON FORMATION OF THEIR SPATIAL ORGANIZATION AND CONFORMATION MOBILITY

L.I. VELIYEVA, E.Z. ALIYEV
Baku State University, Az-1148, Z.Khalilov str., 23
Lala_Veliyeva@rambler.ru

The spatial structure of *Leu*-callatostatines 1 and 2 is studied by the method of theoretic conformation analysis. The stability quantitative evaluation of possible molecule conformation states based on calculation of intramolecular conformation energy value in conditions of dipolar medium is carried out.

Keywords: neuropeptides; structure; conformation analysis.
PACS: 87.80.-y

INTRODUCTION

The search and purposeful synthesis of compounds used for regulation of pest number is the one of actual problems in modern science. The neuropeptides synthesized by neurosecretory cerebrum cells of insect different types, in particular, *Calliphora Vomitoria* [1-3] belong to such compounds. The neuropeptides inhibit the synthesis and extraction of juvenile hormones in process of insect ontogenesis; take participation in neurotransmission and regulation of nervous system functions. The study of molecular mechanism basis of neuropeptide influence and formation of effective analogues of these compounds with prolonged action effect is the important aspect of investigations of neuropeptide functional activity. The study of spatial structure and conformation properties of *Leu*-callatostatines 1 and 2 is the aim of the present investigation. The neuropeptide chemical structure and calculation scheme of conformation states grown gradually di-, three- and penta-peptide fragments of molecules is given in fig.1.

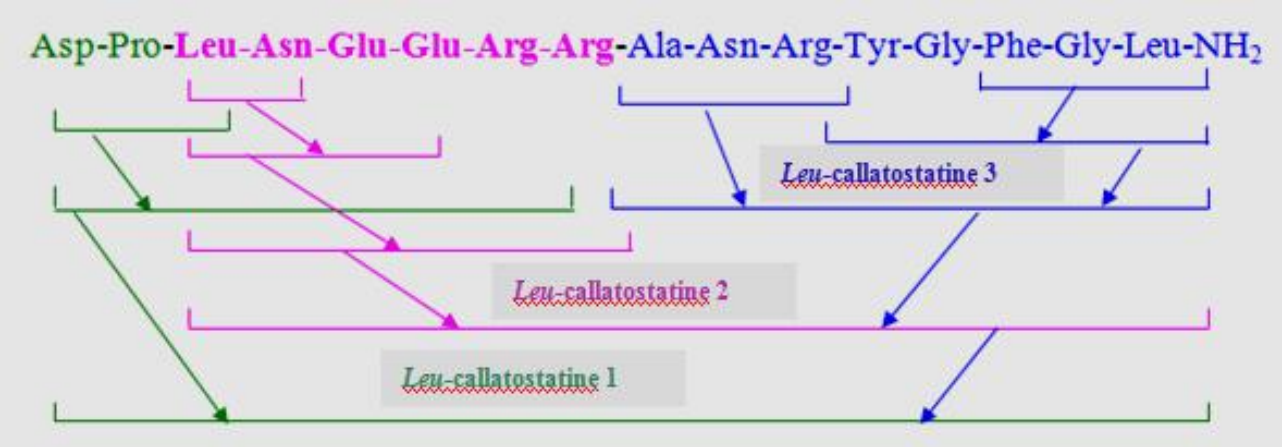

Fig.1. The calculation scheme of *Leu*-callatostatine molecule.

As it is seen from the figure, *Leu*-callatostatine 1 and *Leu*-callatostatine 2 are hexa- and tetra-decapeptide compounds including the eight amino-acid residuals of *Leu*-callatostatine 3. That's why the investigation of their spatial structure is carried out on the base of calculation results obtained for *Leu*-callatostatine 3 and molecule fragments according to scheme given in fig.1. The number decrease of initial structural approximations at conformation analysis of more complex fragments and whole molecule is the aim of the calculations of low-energy conformation states of di-, three- and other peptide sections and their overlapping fragments according to this scheme.

THE CALCULATION METHOD

The low-energy conformation molecule states are established by the way of minimization of total conformation energy in force field of atom-atom potential functions. At energy calculations the non-valence (E_{nv}) and electrostatic (E_{el}) atom interactions, hydrogen bonds (E_h) and torsion contributions (E_{tors}) for description of which the semiemperical potential functions given in works [4,5] are used. The calculations are carried out within framework of strong valence scheme, i.e. at fixed values of valence bond lengths and valence angles of amino-acid residual including in molecule chemical structure. The used system of potential functions and

131 H.Javid ave, AZ-1143, Baku
ANAS, G.M.Abdullayev Institute of Physics
E-mail: jophphysics@gmail.com

computational programs are approved for the big number of peptides and proteins by the authors of the given work and other investigators [7-10].

The parameterization given in works [4-6] is used for water surrounding modeling. The hydrogen bond energy is estimated with the help of Morse potential at dissociation energy of hydrogen bond equal to 1,5 kcal/mol corresponding to distance of bond NH…OC r=1.8Å for water solutions. The dielectric constant value is takes as 10 [4,5]. The conventional classification of peptide structures [6] is used at discussion of calculation results. The choice of structural variants at calculation of separate peptide conformations is carried out on the base of known values of dihedral angles (φ и ψ) corresponding to low-energy ranges of conformation card of R,B,L and P for each monopeptide. The count of dihedral angles corresponds to international nomenclature [6].

THE CALCULATION RESULTS

LEU-CALLATOSTANIE 2.

The general number of structural variants for *Leu*-callatostatine 2 is made up on the base of combination of 38 structures of *Leu*-callatostatine 3 and 17 low-energy conformation states of N-end hexapeptide overlapping by Ala^7 residual. The calculation results of hexapeptide fragments are given in tables 1 and 2 (the calculation intermediate stages aren't given because of the procedure uniformity of calculative experiment). They include 10 low-energy conformations from 31 acceptable ones for such shape fragments the relative energy of which satisfies to condition $E_{rel.} \leq 6$ kcal/mol.

Table 1.

The energy distribution of optimal conformations in shapes of Leu^1-Arg^6 fragment of *Leu*-callatostatine 2.

№	shape	Energy interval $E_{rel.}$ (kcal/mol)				
		0 ÷ 1	1 ÷ 2	2 ÷ 3	3 ÷ 4	4 ÷ 5
1.	*ffffee*	-	-	1	-	1
2.	*ffffef*	1	-	-	-	-
3.	*ffefee*	-	-	-	1	-
4.	*ffefef*	-	-	-	-	1
5.	*ffeffe*	1	-	1	-	3
6.	*ffefff*	-	-	1	-	1
7.	*ffeeff*	-	-	-	1	-
8.	*efefef*	-	-	-	-	1
9.	*efeffe*	-	-	1	-	-
10.	*feffff*	-	-	-	-	1
11.	*fefffe*	-	-	-	-	1
12.	*feffef*	-	-	-	-	1

Table 2.

The low-energy conformational states of *N*-end hexapeptide fragment of *Leu*-callatostatine 2.

shape	conformation	Energy contributions (kcal/mol)				
		E_{nv}	E_{el}	E_{tors}	E_t	E_{rel}
ffeffe	$R_2R_{11}B_1R_2B_1L_3B$	-33.97	-2.62	5.79	-30.80	**0.00**
	$R_2R_{11}B_1R_2B_1L_3R$	-32.12	-2.34	5.68	-28.78	2.02
ffffef	$R_2R_{11}R_3R_2R_3L_2L$	-37.90	2.17	5.54	-30.19	0.61
ffffee	$R_2R_{11}R_3R_2R_3L_2B$	-36.97	2.90	5.83	-28.24	2.56
	$R_2R_{11}R_3R_2R_3L_2R$	-35.27	2.71	6.10	-26.46	4.34
ffefef	$R_2R_{11}B_1R_2R_3L_2L$	-31.39	0.73	4.74	-25.93	4.87
ffefff	$R_2R_{11}B_1R_2B_1L_2L$	-29.75	-1.07	4.58	-26.24	4.56
	$R_2R_{11}B_1R_2B_1L_3L$	-31.99	-2.22	5.79	-28.42	2.38
efefef	$B_2R_{31}B_3R_2R_3L_2L$	-31.20	1.46	3.53	-26.21	4.59
efeffe	$B_2R_{31}B_3R_2B_3L_3R$	-26.64	-2.14	5.30	-28.47	2.33
fefffe	$R_2B_{11}R_3R_2B_3L_3B$	-32.23	1.91	4.44	-25.88	4.92
feffff	$R_2B_{11}R_3R_2B_3L_3L$	-32/23	1.99	4.27	-25.97	4.83
feffef	$R_2B_{11}R_3R_3B_2R_2R$	-33.00	2.18	9.05	-26.13	4.67

The minimization of conformational energy of whole neuropeptides is carried out at variation of 81 dihedral angles in main and side chains of residuals for different type structures of molecule peptide composition. Only 47 conformations have the energy the value of which satisfies to condition $\Delta E_{rel.} \leq 10$ kcal/mol from 285 calculated conformations.

All of them present the combination of more beneficial states of Leu^1-Arg^6 and Ala^7-Leu^{14} fragments of *Leu*-callatostatine 2 molecule (see tables 2 and 3) in spite of the strong difference in energies of obtained structures.

Table 3.

The distribution of low-energy conformations on shapes of neuropetide *Leu*-callatostatine 2

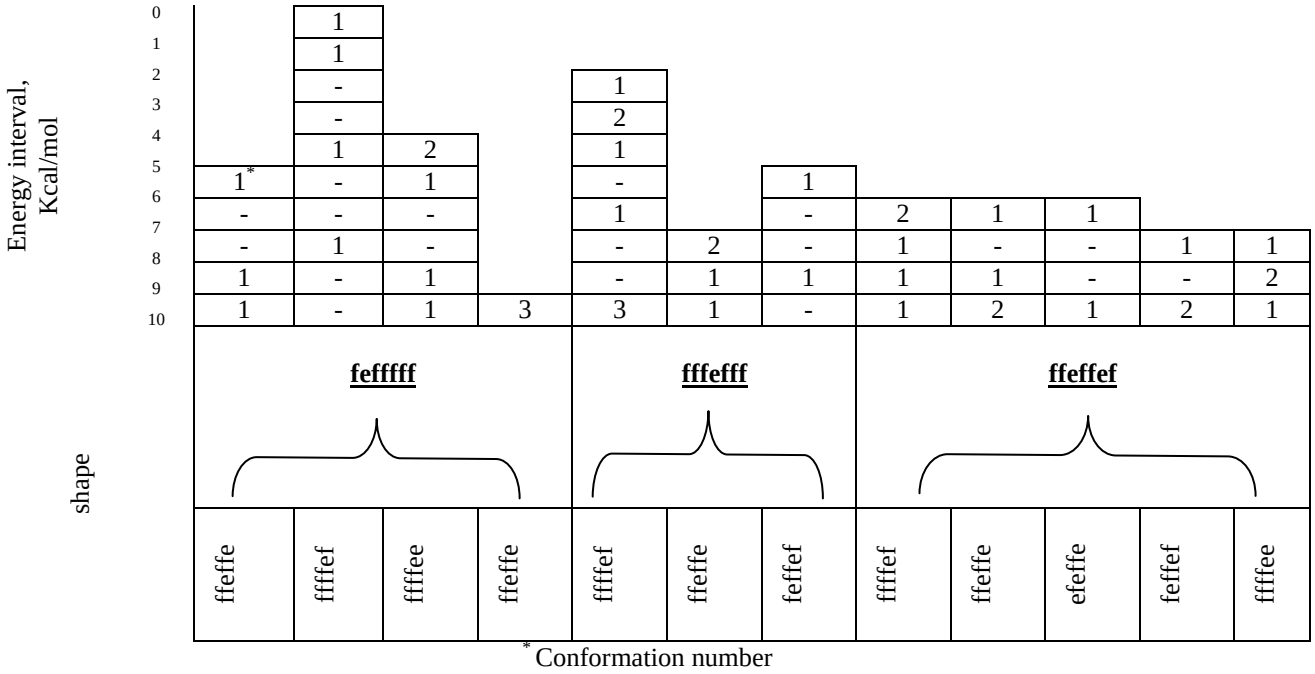

The formation of far interactions [8] which don't destroy the interresidual interactions formed on free fragments of calculated molecule is the important factor in formation of neuropeptides spatial organization. Thus, the necessity in coincidence of near, middle and far interactions [7,8] promoting to step-by-step oligopeptide packing into native conformation is confirmed. The side chains of amino-acid residuals, from orientation of which depends the rapid convergence of conformational energy in minimization procedure and finding of its global minimum. That's why the finding of local minimums in neighborhood of obtained values of conformational energy by the way of construction of conformational card series φ-ψ and χ_i - χ_{i+1} is the important stage.

They allow us to eliminate the appearing destabilizing contacts at fragment integration in some cases and make the energy minimization at variation of variable limited number.

The investigation results of *Leu*-callatostatine 2 spatial construction are given in tables 3 and 4. The distribution of neuropeptide low-energy conformations in dependence on peptide framework structural type, i.e. the conformation classifications by shapes is given in first table. As it is seen from this table not all combinations of low-energy fragments Leu^1-Arg^6 and Ala^7-Leu^{14} lead to formation of energy profitable and steric accessible states of neuropeptide.

The stability of calculated structures in dependence on stereochemical disposition of amino-acid residuals and their side chains in linear sequence of neuropeptide is determined by the presence of ordered regions in its spatial organization. All neuropeptide conformations can be classified in four groups due to such character elements.

I group consists in the conformations having two regular sections placed on neuropeptide opposite ends. They are characterized by formation of two turns of α-spiral divided by Arg^6 - Arg^9 section having the charged side chains of arginine residuals. The analysis of interresidual interactions in such conformations shows that side chains locate on the surface of neuropeptide compact structure and don't take participation in stabilization of their spatial structure. The four low-energy conformations of *ffffeffeffff* and *ffffeefeffff* shapes in group I differ by the peptide chain state in *Ala* and different orientations of Arg^6 and Arg^9 side chains. The best neuropeptide conformation ($E_{rel.}$= 0 kcal/mol, table 4) consists in α-spiral conformation of *Leu*-callatostatine 3 and one from low-energy conformations of Leu^1-Arg^6 hexapeptide.

The low-energy conformations of second group contain three α-spiral sections in neuropeptide structure and differ by conformational state of residuals in sixth (Arg^6) and eleventh (Gly^{11}) positions of amino-acid linear sequence. The glycine doesn't contain the side chain in difference from rest residuals, that's why *C*-end α-spiral fragment is presented by two possible orientations of relatively less mobile *N*-end section. The difference on conformation relative energy of this group varies in limits 0-1 kcal/mol. The surface of compact structures of this neuropeptide group is represented by only one positively charged side chain of Arg^6 residual. That's why such structures should have the less reactivity in comparison with I group conformations.

Table 4.

The low-energy conformational states of *Leu*-callatostatine 2 neuropeptide and contributions from non-valence, electrostatic and torsion interactions.

Classifi-cation by groups	IIIShape	Conformation	Energy contributions (kkal/mol)				
			$E_{nv.}$	$E_{el.}$	$E_{tors.}$	E_t	$E_{tel.}$
I	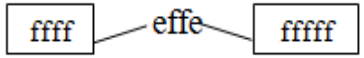	$R_2R_{11}R_3R_2B_3R_2RB_{11}R_2B_3PB_2PB_{21}$ $R_2R_{11}R_3R_3B_1R_2RB_{11}R_2B_3PB_2PB_{21}$	-65.60 -65.29	4.15 3.12	24.51 26.43	-36.94 -35.74	**0.0** 1.2
	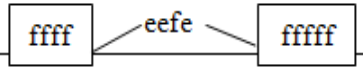	$R_2R_{11}R_3R_2R_3L_2BL_{11}R_2B_3PB_2PB_{21}$ $R_2R_{11}R_3R_2R_3L_2RB_{21}R_2B_3PR_2RR_{21}$	-65.45 -63.47	4.21 2.98	29.10 28.75	-32.14 -31.74	4.6 5.2
II	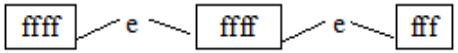	$R_2R_{11}R_3R_2B_1R_2RR_{11}R_2R_3PB_2PB_{32}$ $R_2R_{11}R_3R_2B_1R_2RR_{11}R_2R_3PB_2PB_{31}$ $R_2R_{31}R_3R_3B_3R_2RR_{11}R_2R_3PB_2PB_{32}$ $R_2R_{31}R_3R_3B_3R_2RR_{11}R_2R_3PB_2PB_{31}$	-65.42 -65.42 -65.71 -64.37	3.77 3.12 3.56 2.11	27.21 28.96 29.01 29.52	-34.44 -33.34 -33.14 -32.74	2.3 3.6 3.8 4.2
III	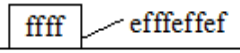	$R_2R_{11}R_3R_2B_3R_2RR_{22}B_3B_1PR_1PR_{32}$ $R_2R_{11}R_3R_3B_1R_2RR_{21}B_3B_1PR_1PR_{32}$	-60.84 -64.63	2.60 4.27	28.00 30.62	-30.24 -29.74	6.7 7.2
IV	ffeffeffeffef	$R_2R_{11}B_1R_2B_1L_3BL_{22}L_1B_1PR_1PR_{31}$ $R_2R_{11}B_1R_2B_1L_3RR_{22}B_3B_1PR_1PB_{21}$ $R_2R_{11}B_1R_2B_1L_3RR_{32}B_3B_1PR_1PR_{32}$	-60.08 -59.99 -59.67	2.70 2.74 3.05	28.64 29.41 29.28	-28.74 -27.84 27.34	8.2 9.1 9.6
	efeffeffeffef	$B_2R_{31}B_3R_2B_3L_3RR_{22}B_3B_1PR_1PB_{21}$ $R_2R_{11}B_1R_2B_1L_3RR_{32}B_1B_1PR_1PB_{32}$	-61.25 -60.54	2.98 3.11	31.13 30.39	-27.14 -27.04	9.8 9.9

* Note: The energy from formation of hydrogen bonds is included in E_{nv}.

The conformations, characterizing by α-spiral conformation of *N*-end penta-peptide fragment are combined in group III. They present by big number of conformational states on *C*-end fragment, but only two of them have the energy the value of which doesn't exceed the energy of neuropeptides global conformation more than 10 kcal/mol.

Those conformations which don't consist in the strong nucleations or stable regular elements in their spatial organization form the fourth group. The low-energy representatives of such structures are given in table 4.

LEU-CALLATOSTATINE 1.

As the difference in primary structure of *Leu*-callatostatine 1 is caused by the presence of two Asp^1 and Pro^2 residuals on *N*-end fragment of the last neuropeptides, then the investigation of its spatial organization leads to step-by-step residual generation of linear chain of *Leu*-callatostatine 2. The serially attachable residuals *Pro* and *Asp* are considered in field of all structures of four types obtained by us for *Leu*-callatostatine 2. Moreover, it is taken into consideration that the proline residual not only limits the region of acceptable conformational states for Asp^1 (only *B* and *L* regions of conformational space are possible for it), but it itself has the limited conformational mobility in *B* and *R* regions. The total energy minimization of *Leu*-callatostatine 2 neuropeptides is carried out for 15 conformational states of whole molecule. The calculated results are summarized and the energy characteristics of 6 conformations of *Leu*-callatostatine 1 neuropeptide are given in table 5.

Table 5.

The low-energy conformational states of *Leu*-callatostatine 1 molecule.

shape	conformation	Energy contributions (kcal/mol)				
		E_{nv}	E_{el}	E_{tors}	E_t	E_{rel}
eeffffeffffff	$B_1BR_2R_{11}R_3R_2B_3R_2RB_{11}R_2B_3PB_2PB_{21}$	-75.93	11.22	16.90	-47.82	0.00
eefffeefffff	$B_3BR_2R_{11}R_3R_2R_3L_2BL_{11}R_2B_3PB_2PB_{21}$	-75.42	15.76	12.15	-47.51	0.31
eefffeffffefff	$B_1BR_2R_{11}R_3R_2B_1R_2RR_{11}R_2R_3PB_2PB_{32}$	-74.34	15.11	11.72	-47.50	0.32
effffeffffff	$B_2RR_2R_{11}R_3R_2B_3R_2RB_{11}R_2B_3PB_2PB_{21}$	-72.40	15.32	12.32	-44.71	3.11
effffeefffff	$B_2RR_2R_{11}R_3R_2R_3L_2BL_{11}R_2B_3PB_2PB_{21}$	-79.20	19.63	12.23	-47.34	0.48
effffeffffefff	$B_2RR_2R_{11}R_3R_2B_1R_2RR_{11}R_2R_3PB_2PB_{32}$	-76.16	20.17	12.27	-43.73	4.09

They reveal the succession of structural types of *Leu*-callatostatine 2. The conformational stability is mainly caused by dispersion contacts between residuals. The low-energy and interconnected changes of side chain conformations are possible in narrow limits their values that confirm the fact that their optimal positions are defined not by steric limits but by interactions with each other.

[1] *H. Duve, A.H. Johnsen, A.G. Scott, C.G. Yu, K.J. Yagi, S.S. Tobe, and A. Thorpe.* "Callatostatins: Neuropeptides from the blowfly Calliphora vomitoria with sequence homology to cockroach allatostatins" (1993) Proc. Natl. Acad. Sci. USA, **90**, 2456- 2460.

[2] *H. Duve, A.H. Johnsen, J.L. Maestro, A.G. Scott, P.D. East, A. Thorpe.* "Identification of the dipteran Leu-callatostatin peptide family: the pattern of precursor processing revealed by isolation studies in Calliphora vomitoria" (1996) Regul.Pept., **67**, 11-19.

[3] *H. Duve, A. Thorpe.* "Distribution and functional significance of Leu-callatostatins in the blowfly Calliphora vomitoria" (1994) Cell Tissue Res., **276**, 367-379.

[4] *F.A. Momany, R.F. McGuire, A.W. Burgess, H.A. Scheraga.* "Energy parameters in polypeptides: VII. Geometric parameters partial atomic charges, nonbonded interaction for naturally occurring amino acid" (1975) J.Phys.Chem., **79**, 2361-2381.

[5] *E.M. Popov.* The Structural Organization of Proteins (in Russian), Nauka, Moscow, 1989, 352 pp.

[6] IUPAC-IUB Commision on Biochemical Nomenclature Abbreviations and symbols for description of conformation of polypeptide chains (1974) Pure Appl. Chem., **40**, 291-308.

[7] *T.K. Hayes, X.C. Guan, V. Johnson, A. Strey, S.S. Tobe.* "Juvenile-hormone binding components of locust fat-body". ***Arch. Insect Biochem. and Phys.,*** 1995, v.28, N.3, p.291-309.

[8] *D. Veelaert, L. Schoofs, S.S. Tobe, C.G. Yu, H.G.B. Vullings, F. Couillaud, A. Deloof.* "Biosynthesis and release of juvenile-hormone during the reproductive cycle of the ring-legged earwing". ***Comparative Biochem.and Phys. (pharmocology, toxicology and endocrinology),*** 1995, v.110, N.3, p.241-251.

Recevied: 12.04.2016

ISSN 1028-8546

2016, Vol. XXII, № 2
Section: En

CONTENTS